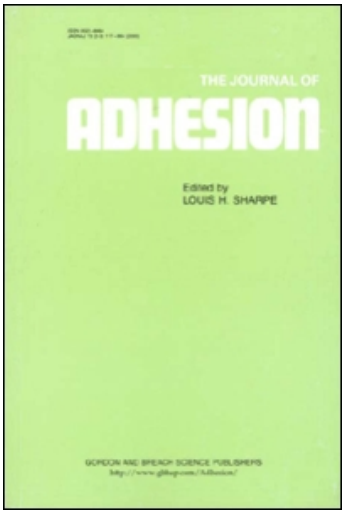

The Journal of Adhesion
Publication details, including instructions for authors and subscription information:
http://www.informaworld.com/smpp/title~content=t713453635

Adhesive and Rheological Properties of Lightly Crosslinked Model Acrylic Networks

A. Lindner[a]; B. Lestriez[a]; S. Mariot[a]; C. Creton[a]; T. Maevis[b]; B. Lühmann[b]; R. Brummer[c]
[a] Laboratoire de Physico-Chimie des Polymères et Milieux Dispersés, E.S.P.C.I., Paris, France [b] Tesa AG, R&D Raw Materials—Polymer Physics, Hamburg, Germany [c] Beiersdorf AG, Analytics Department, Hamburg, Germany

To cite this Article Lindner, A. , Lestriez, B. , Mariot, S. , Creton, C. , Maevis, T. , Lühmann, B. and Brummer, R.(2006) 'Adhesive and Rheological Properties of Lightly Crosslinked Model Acrylic Networks', The Journal of Adhesion, 82: 3, 267 — 310
To link to this Article: DOI: 10.1080/00218460600646594
URL: http://dx.doi.org/10.1080/00218460600646594

The Journal of Adhesion, 82:267–310, 2006

ISSN: 0021-8464 print/1545-5823 online
DOI: 10.1080/00218460600646594

Taylor & Francis
Taylor & Francis Group

Adhesive and Rheological Properties of Lightly Crosslinked Model Acrylic Networks

A. Lindner
B. Lestriez
S. Mariot
C. Creton
Laboratoire de Physico-Chimie des Polymères et Milieux Dispersés, E.S.P.C.I., Paris, France

T. Maevis
B. Lühmann
Tesa AG, R&D Raw Materials—Polymer Physics, Hamburg, Germany

R. Brummer
Beiersdorf AG, Analytics Department, Hamburg, Germany

The viscoelastic and adhesive properties of a series of model, lightly crosslinked acrylic polymer networks have been investigated. The model networks were statistical copolymers of 2-ethyl-hexyl acrylate and acrylic acid or terpolymers of 2-ethyl-hexyl acrylate, acrylic acid, and stearyl acrylate synthesized in solution. All were lightly crosslinked after the polymerization was completed to obtain typical properties of pressure-sensitive adhesives. The bulk rheological properties of the networks were characterized by dynamical mechanical spectroscopy and in uniaxial extension. Their adhesive properties were tested with an instrumented probe tester fitted with a cylindrical steel probe. The presence of acrylic acid in the copolymer caused an increase in both elastic modulus and resistance to interfacial crack propagation characterized by the critical energy-release rate $\mathcal{G}_c$ and the incorporation of stearyl acrylate caused a decrease in both modulus and $\mathcal{G}_c$. In both cases, however, the modification of $\mathcal{G}_c$ controlled the overall behavior. The analysis of the nonlinear elastic properties of the adhesives with the Mooney–Rivlin model provided new insights on the role played by the ratio

Received 4 October 2005; in final form 13 February 2006.
One of a collection of papers honoring Hugh R. Brown, who received the Adhesion Society Award for Excellence in Adhesion Science, Sponsored by 3M, in February 2006.
Address correspondence to Costantino Creton, Laboratoire de Physico-Chimie des Polymères et Milieux Dispersés, E.S.P.C.I., 10, Rue Vauquelin, 75231 Paris Cedex 05, France. E-mail: costantino.creton@espci.fr

between entanglements and crosslink points in controlling the formation and extension of the bridging fibrils observed upon debonding.

Keywords: Acrylate; Acrylic acid; Adhesion, Fracture; Probe tack; PSA; Rheology

1. INTRODUCTION

Self-adhesive materials and products, also called pressure-sensitive-adhesives (PSAs), are becoming increasingly popular for industrial fastening applications where a permanent bond is necessary but no great mechanical strength is required. They are safe to apply for the user because they are solventless, and they allow precise positioning and no overflow of adhesive because of their solid character [1,2].

In general terms PSAs are soft (modulus E below 0.1 MPa) viscoelastic solids composed of a lightly crosslinked high-molecular-weight polymer, which is the backbone of the structure, and one or more low-molecular-weight additives, which typically adjust viscoelastic properties and dilute the entanglement network if need be [1]. This combination of properties can be conveniently and cheaply obtained with three families of polymers: acrylic statistical copolymers, styrenic block copolymers, and natural rubber. Natural rubber–based PSAs were the first to be developed and remain used today mainly for general purpose applications. Adhesives based on styrene–isoprene–styrene block copolymers are processable without solvent above the temperature of order–disorder transition, due to their physically and reversibly crosslinked network of hard styrene domains [3]. However, both of these types of PSA have the disadvantage of a poor environmental stability and tend to degrade under thermooxidative or UV exposure. On the other hand, PSAs based on acrylic random copolymers do not allow such a precise control of the structure but are stable over a wide range of temperatures, and their properties can be tuned by a suitable choice of monomers, degree and type of crosslinking, and formulation. Furthermore, acrylic adhesives display adhesive properties without any additives.

In terms of manufacturing, PSA are typically coated on substrates as 20–100-μm-thick films by three main methods: coating from latex, coating from a solution, and coating from the melt. The first two methods are mainly used for acrylic adhesives and the last method is the method of choice for block copolymer-based adhesives.

Depending on the method, the type of acrylic adhesive which is obtained is different. Coating from latex is economically more interesting because of low viscosities and the absence of organic solvents, but

typically molecular control of the structure of the adhesive is more difficult, and residual surfactants and additives, which are necessary to synthesize and stabilize the latex, can be detrimental to the final properties of the dry film. Despite environmental pressures, coating from solution is still popular for high-end applications, because the molecular structure of the adhesive can be better controlled during the synthesis step and fewer unwanted impurities are left in the adhesive.

Acrylic PSA, even coated from solution, remain complex materials that do not possess a well-defined molecular structure but rather a broad polydispersity in terms of molecular weight, molecular weight between crosslinks, and sometimes monomer composition. This has significantly complicated the task of relating specific changes in the molecular structure of the adhesive to adhesive performance. Most studies on acrylic PSAs have focused on finding empirical correlations between monomer composition, synthesis conditions, and final properties as tested by the user. Such studies were first performed on solution acrylics [4–6] and more recently on acrylic adhesives prepared from latexes [7–10]. In the more recent emulsion acrylic studies, the effect of changing molecular weight and degree of crosslinking [9, 11–13], as well as the effect of changing the nonpolar monomer composition [14] or particle structure [10], was systematically investigated. Unfortunately, however, the information that can be drawn from these studies is often difficult to interpret. Changes in monomer composition lead to changes in gel fraction and molecular-weight distribution, which have a profound effect on properties and are hard to separate from the effect of the monomer itself. Furthermore, some monomers such as acrylic acid modify both the surface and the bulk properties of the adhesive [4]. In the case of emulsion polymers, the use of surfactants and the process of drying and coalescence of the latex particles adds another complication and has an influence on the adhesive properties [15].

Furthermore, adhesive properties of PSAs have been mainly investigated with standard industry tests such as the peel test. Although links were established between the measured peel force and the linear viscoelastic properties of the adhesives [16–18], these studies also showed that the actual detachment of an adhesive layer from a substrate occurs by a very significant and inhomogeneous deformation of the entire layer, which forms a fibrillar structure [16,17,19–21] bridging the backing and the substrate. This type of deformation can clearly not be approximated by a simple linear elastic fracture mechanics approach and requires a more microscopic approach to the deformation mechanisms. The fibrillar structure that we observed is composed of highly oriented polymer chains and can be compared (at an entirely different length scale) with the oriented structure found

in polymer crazes [22]. The conditions under which this structure is formed can be more conveniently investigated with a probe test, which in essence performs a tensile test in the thickness direction of a thin film [23]. The combined use of the full stress–strain curve of the probe test and an *in situ* observation of the deformation mechanisms of the adhesive layer [24,25] has led to significant advances in the understanding of the criteria leading to the formation and failure of the fibrillar structure in PSA for block copolymer-based PSAs [26–28] and emulsion acrylics [24]. It has not yet been used extensively to investigate the effect of controlled changes in molecular structure on the adhesive properties of acrylic PSAs synthesized from solution. The goal of this article is twofold: first, to investigate, with the most advanced methods, the effect on the material properties of incorporating a highly polar comonomer (acrylic acid) and a nonpolar, low-surface-tension comonomer (stearyl acrylate) in a standard acrylate homopolymer typically used for PSA; and second, to contribute to the understanding of the complex relationship between the viscoelastic properties of the adhesive and its adhesive properties on a substrate.

To achieve these goals, we work with a family of model acrylic statistical copolymers, polymerized in solution, which possess PSA properties without any additives. The main variables were the copolymer compositions. All copolymers were based on the 2-ethyl-hexyl acrylate monomer, with controlled additions of acrylic acid and stearyl acrylate. The average molecular weight and molecular-weight distribution of the uncrosslinked polymers were kept constant for all compositions. Because the molecular weight is such an important parameter, we also tested a control sample where the molecular weight was simply halved. This additional sample was not tested to study in the detail the effect of a change in molecular weight but to emphasize qualitatively those properties that would be greatly influenced even by a modest molecular-weight change.

Our approach is as follows:

1. We have synthesized a series of acrylic model PSAs from solution with careful control of their molecular-weight distribution and systematic variations in monomer composition. All PSAs have then been postcrosslinked with the same amount of crosslinking agent.
2. Rheological properties in the small strain regime have been characterized with a parallel plate rheometer.
3. Nonlinear elastic properties have been characterized with a tensile test for selected acrylic adhesives.
4. Adhesive properties and mechanisms of debonding have been characterized with an instrumented probe tack test.

2. MATERIALS AND METHODS

2.1. Materials

The model adhesives used in this study consist of two series of acrylic copolymers based on 2-ethyl-hexyl acrylate (2-EHA) as base monomer (see Figure 1). The first series contains as comonomer increasing amounts (2 wt%, 4 wt%, and 8 wt% corresponding to 5, 10, and 18 mol%) of acrylic acid (AA), whereas the second series contains 2 wt% (5 mol%) AA and increasing amounts (10 wt% and 30 wt% corresponding to 6 and 19 mol%) of stearyl acrylate (StA). The proportions were chosen to give nearly identical mole fractions of comonomer for AA and StA. However, because conventionally the amount of copolymer is given in weight fraction, we have stuck to that naming convention in this article. The adhesive with 2 wt% AA was synthesized also in a lower-molecular-weight version. Adhesives are referred to as 2AA, 4AA, and 8AA for the AA series; as 2AA10StA and 2AA30StA for the StA series, and LOW for the 2AA with a lower-molecular-weight polymer, respectively. All copolymers were synthesized *via* free radical polymerization in solution and exhibit an average molecular weight of $M_w \approx 1200-1500$ kg/mol and a polydispersity index $PDI = M_w/M_n \approx 7-9$ (a special GPC column, Linear One, Polymer Standard Service GmbH, Mainz, Germany), for high molecular weights and polystyrene standards was used for calibration). Special care was taken to obtain as little variation as possible for the molar weight and molar-weight distribution of the copolymers. The LOW sample had a molecular weight about half that of the series. The molecular properties of the base polymers are summarized in Figure 1 and in Table 1.

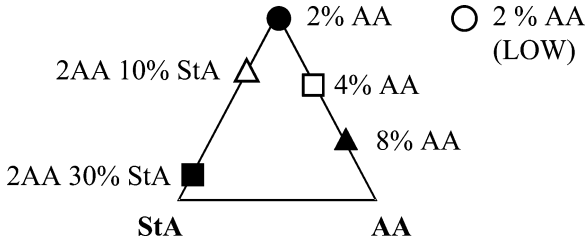

FIGURE 1 Copolymer composition and molecular properties of the model acrylic networks used. All adhesives are based on the 2-ethyl-hexyl acrylate monomer with controlled addition of acrylic acid (AA) and stearyl acrylate (StA). Molecular weight: $M_w = 1200$–1500 kg/mol (except LOW: M_w halved); polydispersity $P_D = M_w/M_n = 7$–9; crosslinking 0.4% Ti–chelate; gel content 60% (except LOW).

TABLE 1 Molecular Weight and Polydispersity Index of the Copolymers Before the Crosslinking Step

Monomer composition	M_w [g/mol]	PDI
98% EHA + 2% AA	1.6×10^6	9.2
96% EHA + 4% AA	1.4×10^6	8.0
92% EHA + 8% AA	1.2×10^6	6.5
88% EHA + 2% AA + 10% StA	1.7×10^6	9.3
68% EHA + 2% AA + 30% StA	1.5×10^6	10.3
98% EHA + 2% AA; low m.w.	4.6×10^5	4.5

To become useful PSAs, these polymers need to be lightly crosslinked to reduce creep. Crosslinking was performed here with the addition of 0.4 wt% of Ti-chelate [(Ti-(IV)-bis-acetylacetonato)-diisopropylate], which was added to the organic solution just prior to the coating step.

Films of the dried, crosslinked polymer were obtained by coating the concentrated adhesive solutions onto a 36-μm-thick siliconized release film (siliconized PET) using a semiautomatic lab coater equipped with a standard comma blade. Solvent evaporation was done by storing the freshly coated release film for 60 min at RT (23 ± 2°C, 50 ± 10% rel. hum.) and subsequently for 60 min at $+120$°C to allow the crosslinking. Finally, the open side of the adhesive was covered with a second release film. Samples were stored at least 1 week at RT prior to mechanical and adhesive testing. Crosslinked adhesives after 1 week's storage showed gel contents of ~60% as measured by extraction.

Prior to testing, one of the release films was peeled off, and the adhesive was manually pressed against a 1-mm-thick precleaned standard microscope glass slide. The second release film was then peeled off. Both surfaces of the film have, therefore, been in contact with a siliconized release film. Previous experience with various similar adhesives indicated that silicone transfer to the adhesive surface takes place but only slightly influences adhesive properties (less than 10% loss in peel after 48 h of contact with release liner at $+40$°C and 0.02 MPa contact pressure, and less than 5% Si in adhesive surface using ESCA).

2.2. Probe Tack Test

The mechanics of the probe test have been extensively studied [29–31], and here we only summarize the main features and the main experimental parameters that can be obtained from the method. A schematic view of such a probe test can be seen in Figure 2a. A cylindrical probe is brought into contact with a thin film of adhesive at a given velocity

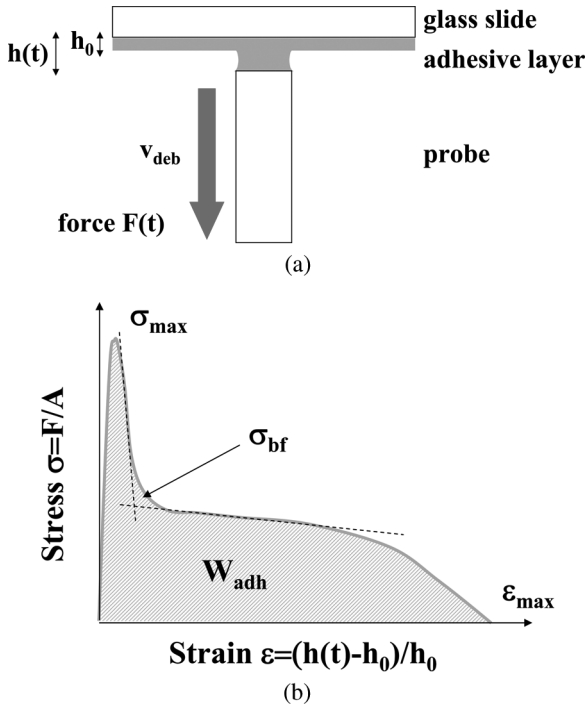

FIGURE 2 (a) Schematic of the experimental setup of the TACK test; (b) typical stress–strain curve obtained from such a test defining the main parameters extracted from the test.

V_{app}. The probe is maintained in contact with the film at a given pressure P_c (the displacement of the probe is actually kept constant while the force relaxes slightly) for a given contact time t_c and is then subsequently removed from the adhesive at a constant debonding speed V_{deb}. During the debonding process, the force F and the displacement h are measured as a function of time. We define h as being the time-dependent thickness of the adhesive layer and h_0 as the initial layer thickness. The measurements can be normalized to obtain an average stress σ *versus* strain ε curve (Figure 2b), where σ is the nominal stress $\sigma = F/A$, with A the area of contact between the probe and the adhesive during the compressive stage, and $\varepsilon = (h - h_0)/h_0$. The shape of the stress–strain curve obtained during such a detachment of the probe from the film can be used to characterize the adhesive performance of the material tested and depends on the rheological properties of the adhesive layer and on the interfacial interactions between the adhesive and substrate. Typical characteristic values that are

extracted from such a curve are the maximum tensile stress, σ_{max}; the stress at the beginning of the plateau, σ_{bf}; the maximum nominal strain to failure, σ_{max}; and the adhesion energy, W_{adh} (the integral under the curve), as shown on Figure 2b. The value of σ_{bf} was defined as the stress level at the intersection between the slope during the cavities expansion (after the peak stress) and the plateau at large strains (see Figure 2b).

The experiments we report were performed using the following experimental conditions: we used a 100-μm-thick adhesive layer deposited on the glass slide. The probe approaches the sample at $V_{app} = 20\,\mu m/s$ and is then maintained in contact with the sample at the contact pressure $P_c = 0.7\,MPa$ for $t_c = 1\,s$. The debonding speed varied between $V_{deb} = 10\,\mu m/s$ and $V_{deb} = 1000\,\mu m/s$. We used a steel probe having a diameter of 6 mm with an average quadratic roughness R_a of 14 nm.

3. RHEOLOGICAL CHARACTERIZATION

3.1 Linear Viscoelastic Properties

3.1.1. Experimental Method

The rheological measurements were conducted with an RDS 700 Series II rheometer (TA Instruments, New Castle, DE, USA). For sample preparation we used a 25-mm-diameter cylindrical form with a 1.5-mm gap and placed it between parallel plates with very low constant normal force. The linear viscoelastic behavior of the acrylic adhesives were found at 1.5% strain for the storage modulus (G') and loss modulus (G''). Master curves were constructed from the time–temperature superposition of data collected at different temperatures. In this article we focus mainly on the frequency–temperature range relevant for the probe tests, *i.e.*, 3–60°C and 0.01–10 rad/s.

3.1.2. Effect of AA Content

The acrylic acid monomer is known to create specific interactions between neighboring chains due to the formation of hydrogen bonds. This increase in the material cohesion strength is clearly perceptible in oscillatory shear at low strains. Figure 3a and 3b shows the results for the storage modulus and tan δ for increasing AA content. The storage modulus increases markedly with AA content over a large range of frequencies. Furthermore, the dissipative character of the material is also observed to shift to lower frequencies with increasing AA content. The shift in T_g is particularly pronounced for the 8AA containing 18 mol% of acid, *i.e.*, almost one monomer in five.

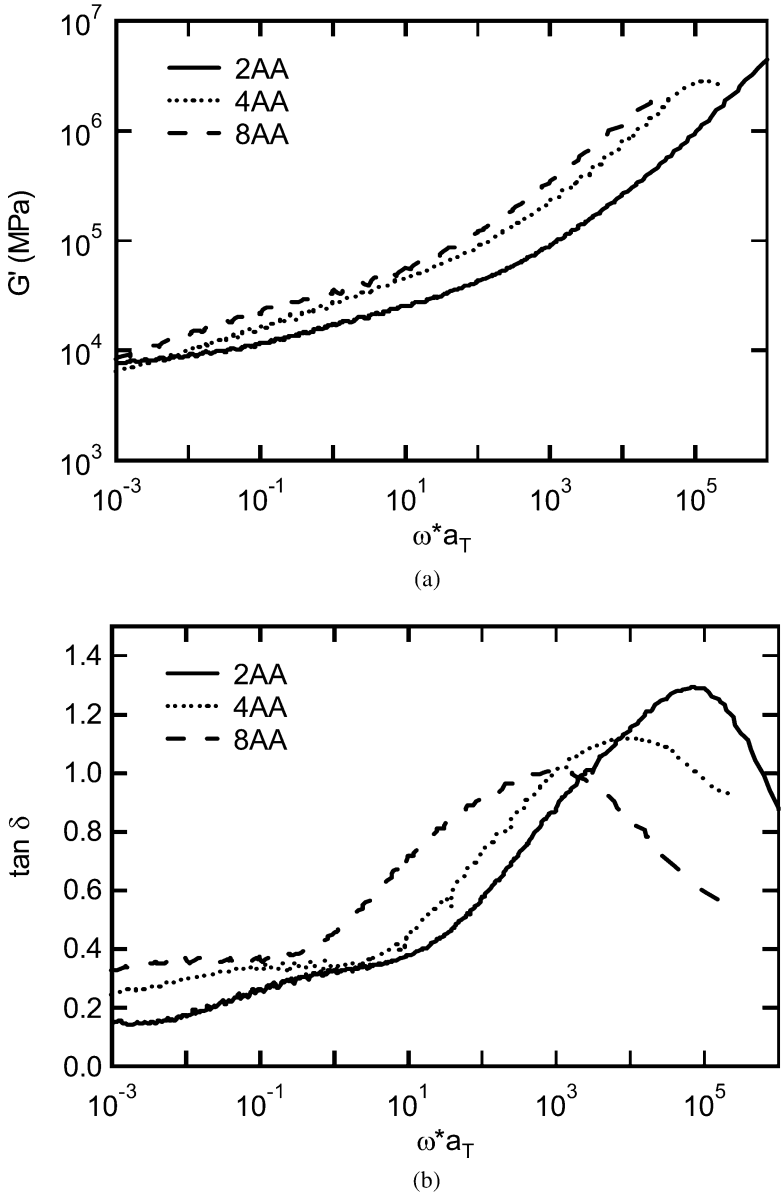

FIGURE 3 Master curves of (a) storage modulus G' and (b) tan (δ) as a function of reduced shear rate for three different adhesives with increasing AA content. Reference temperature: 25°C.

When comparing tests performed at the same temperature and frequency, the net result of adding AA is to make the adhesive stiffer and more dissipative. An alternative way to describe the effect of an increase in AA content in our system would be an increase in the T_g.

3.1.3. Effect of StA Content

The stearyl acrylate monomer is a long side-chain acrylic monomer, which is often used to decrease the surface tension of the adhesive. It also acts as an internal solvent, increasing the average molecular weight between entanglements. This effect is clearly detectable in oscillatory shear. Figure 4a shows that the storage modulus is only modified at low frequencies, compared with the pure 2AA. However, the dissipative character of the 10StA increases compared with 2AA (see Figure 4b) whereas 2AA30StA shows the same behavior as pure 2AA. The T_g seems to be unchanged for all three copolymers. Note that all StA copolymers can crystallize at low temperatures. However, only the 2AA30StA crystallizes at temperatures above 0°C and, thus, rheological experiments were not performed below 25°C to avoid interferences with the crystallization process.

3.1.4. Effect of Molecular Weight

Decreasing the molecular weight of the uncrosslinked polymer has, after crosslinking, only a limited influence on the storage modulus in a wide range of frequencies as can be seen in Figure 5a. At very low frequencies, however, the lower initial molecular weight leads to a significantly lower storage modulus. This result can be explained by the more liquid-like character of the adhesive, because the same wt% of crosslinker was used for a different initial average chain length, therefore resulting in a lower gel content. This leads also to an increase of the dissipative character of the low molecular weight at low frequencies (see Figure 5b).

3.2. NonLinear Elastic Properties

We performed all our tensile tests on a standard tensile-testing machine (JFC TC3, JFC, Villemu sur Tarn, France) adapted to measure large deformations and low forces with a very good resolution (0.5 mN). The samples tested were rectangular with the following dimensions: 1 mm thick (except for the LOW, which had a thickness of 1.6 mm), 4 mm wide, and 15 mm long (length between the clamps). They were prepared at the desired thickness in the same way as the films used for the probe tests.

Tensile tests were performed at room temperature only. The tests were performed at three constant crosshead velocities: 5, 50, and

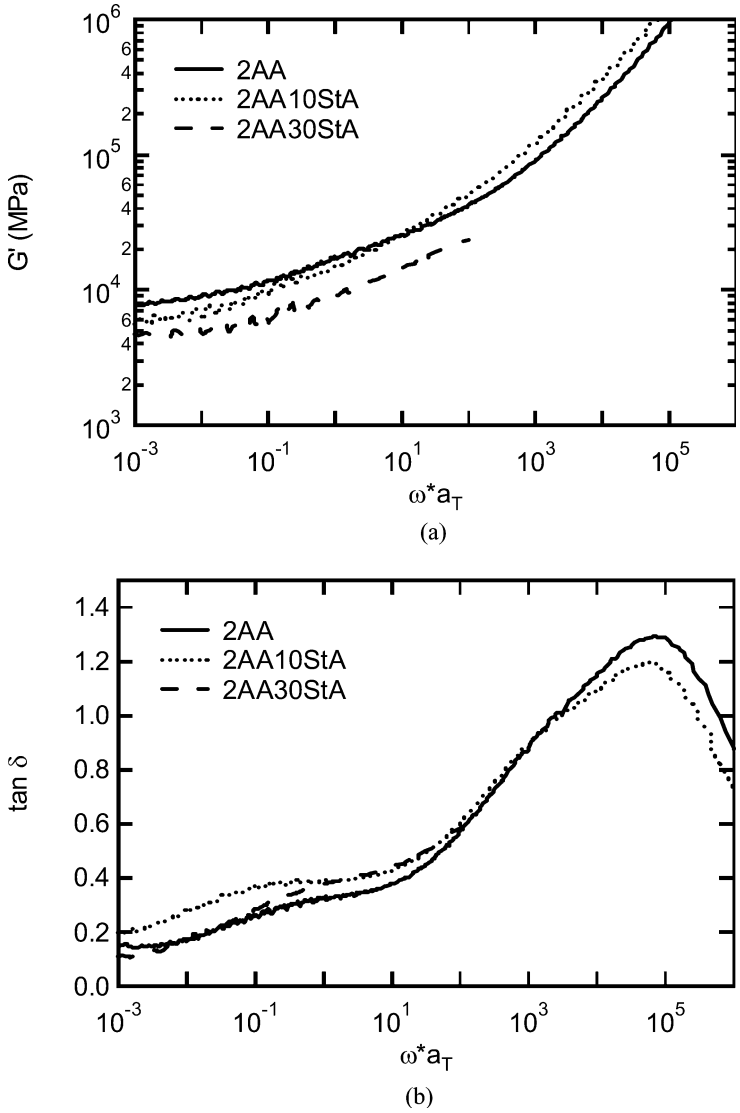

FIGURE 4 Master curves of (a) storage modulus G' and (b) tan (δ) as a function of shear rate for three different adhesives with increasing StA content. Reference temperature: 25°C.

500 mm/min^{-1}. The choice of these velocities was made to approximately replicate the strain rate that the adhesive experiences when it begins to form a fibrillar structure corresponding to initial strain

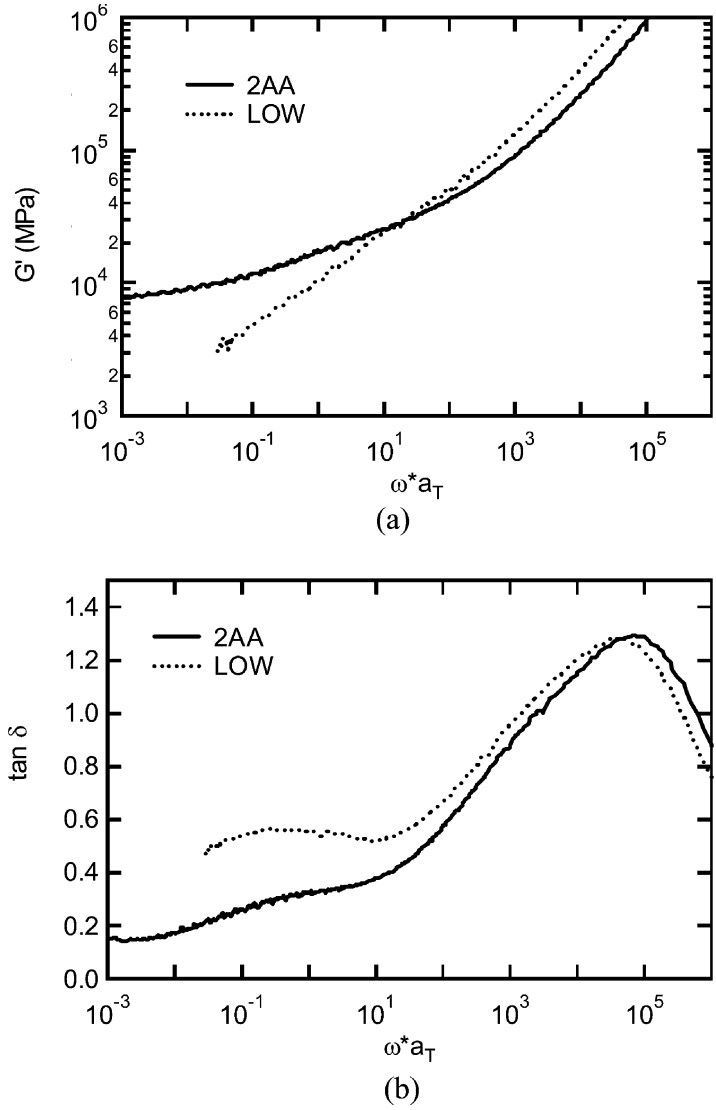

FIGURE 5 Master curves of (a) storage modulus G' and (b) tan (δ) as a function of reduced shear rate for the 2AA and LOW adhesives. Reference temperature: 25°C.

rates of 0.0056 to 0.56 Hz. All tensile tests were repeated twice except for the lowest velocity of $5\,\text{mm}\cdot\text{min}^{-1}$. Reproducibility was good.

It is important to note that tensile tests performed in the large strain regime at constant crosshead velocity do not deform the sample at a constant strain rate. A proper configuration would have called for an exponentially increasing crosshead velocity to compensate for the increase in length of the sample as it is being deformed. This was not possible with our setup, but because our materials show a strong elastic component we feel that a simple tensile test performed at different crosshead velocities already provides most of the information. The influence of different strain rates on our results is discussed in more detail later in this section.

The force F and displacement L data were directly obtained from the tensile-testing machine. Because of the very sticky and soft nature of the adhesive tested, no slippage at the clamps was observed. The nominal stress (σ_N) and the deformation (ε) data were then calculated using the initial values of the width w_0, the thickness e_0, and the height L_0 of the sample:

$$\sigma_N = \frac{F}{w_0 e_0} \qquad \text{and} \qquad \varepsilon = \frac{L - L_0}{L_0}. \tag{1}$$

Typical shapes of nominal stress (σ_N) *versus* strain (ε) tensile curves can be seen in Figure 6 for 2AA at different crosshead velocities V_t. Although the absolute stress values depend on strain rate (with

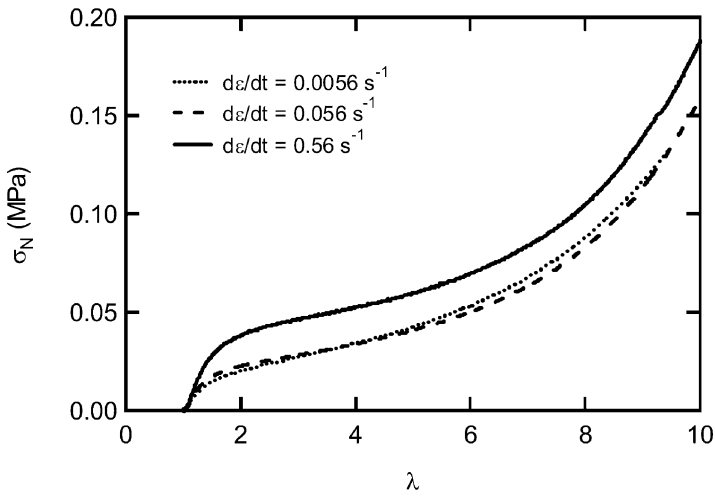

FIGURE 6 Nominal stress σ_N as a function of extension ratio λ for tensile tests of 2AA at different crosshead velocities (5, 50, 500 mm/min) corresponding to different initial strain rates noted on the figure.

$V_t = 500\,\text{mm}\cdot\text{min}^{-1}$ leading to higher values), the overall shape of the curve does not. This holds for all adhesives tested and is indeed the consequence of the elastic character of the PSA.

Furthermore, the tensile behavior is clearly nonlinear for strains higher than 0.5. For the reader accustomed to large strain elasticity in rubbers, the curves of Figure 6 show a very pronounced softening at intermediate strains followed by a pronounced hardening at large strains. This type of nonlinear elastic curve is also found for other families of PSA and is typical of what is required from a PSA [26,28].

Let us now examine the changes brought about by the introduction of a comonomer. Nominal stress *versus* strain curves for the different adhesives at a crosshead velocity of $V_t = 500\,\text{mm/s}$ are shown in Figure 7. Focusing on low strains, only 8AA shows a significantly higher stress level, whereas the other adhesives behave in a similar way. However, at large strains the adhesives are well differentiated: 2AA30StA shows a more pronounced hardening, which is visible at relatively moderate levels of strain, and LOW shows almost no strain hardening in comparison with the other adhesives.

This behavior calls for some comments: The presence of AA in the composition does not by itself change the large strain behavior as much as it does the linear viscoelastic properties. Stress levels are higher, but the shape of the curve is similar. On the other hand, the

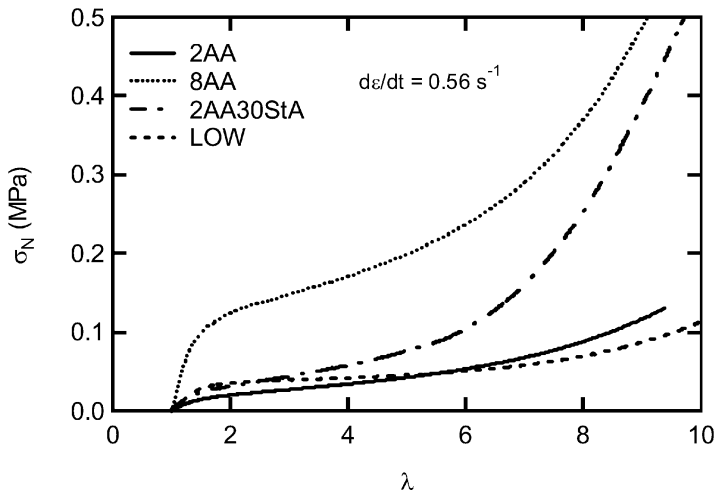

FIGURE 7 Nominal stress σ_N as a function of extension ratio λ for tensile tests of 2AA, 8AA, 2AA30StA, and LOW at a crosshead velocity of 500 mm/min corresponding to an initial strain rate of $0.56\,\text{s}^{-1}$.

introduction of StA does seem to affect both linear viscoelastic properties and large strain properties. The comparison of LOW and 2AA shows that an increase in crosslinking has a direct effect on the strain hardening behavior at large strains. Hence, it is likely that the presence of StA either favors the formation of a higher volume density of hydrogen-bonded interactions (the gel content remains the same), which act mechanically as permanent crosslinks while being soluble in a good solvent, or favors a heterogeneous distribution of crosslinking points (in this case the short segments would control the strain hardening).

A clearer picture of the differences in nonlinear elasticity introduced by the comonomers and the crosslinking comes from the representation of the data in terms of reduced stress. The statistical theory of rubber, also called neo-Hookean elasticity, predicts in uniaxial extension for the nominal stress $\sigma_N = G(\lambda - 1/\lambda^2)$. Hence, it is often interesting to plot the data in terms of the reduced stress defined as $\sigma_R = \sigma_N/(\lambda - 1/\lambda^2)$ with $\lambda = 1 + \varepsilon$ and G the shear modulus. This representation highlights the difference between the experimental data and the statistical theory of rubber elasticity which is itself already nonlinear. Furthermore, because the prediction of the statistical theory does not fit the data above 20% deformation even for standard crosslinked rubbers, it is usual for larger deformations to fit the experimental data with the so-called Mooney–Rivlin constitutive equation, which is presented here in its version for uniaxial tension,

$$\sigma_N = 2\left(C_1 + \frac{C_2}{\lambda}\right)\left(\lambda - \frac{1}{\lambda^2}\right), \tag{2a}$$

$$\Leftrightarrow \sigma_N = 2\left(C_1 + \frac{C_2}{\lambda}\right), \tag{2b}$$

which introduces a λ-dependent deviation from the neo-Hookean case through the parameter C_2.

For this purpose, the reduced stress σ_R was plotted as a function of $1/\lambda$ in Figure 8 for the same conditions as in Figure 7. If one reads the figure from right to left (decreasing $1/\lambda$, increasing λ), one can see that instead of being constant, σ_R decreases until it reaches a minimum at about $1/\lambda = 0.2$ and increases again, illustrating the softening followed by the hardening. σ_R does not increase linearly with $1/\lambda$ over the entire deformation range. However, a linear intermediate part can be seen approximately between inverse strains of 0.3 and 0.7, and we performed fits of the experimental data with the Mooney–Rivlin model within this range.

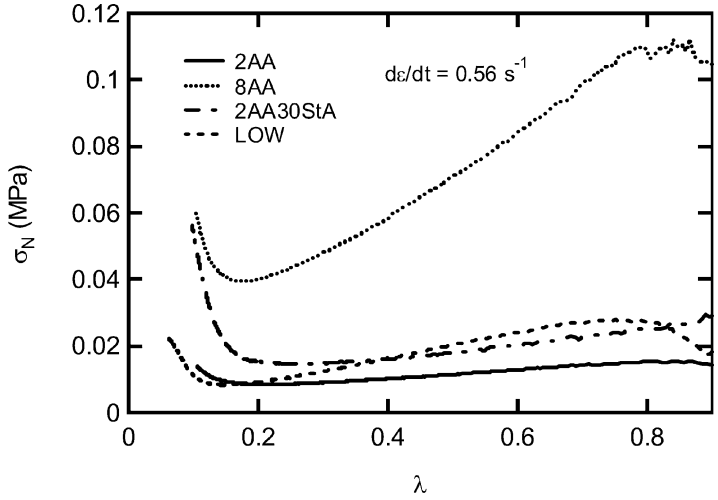

FIGURE 8 Reduced stress σ_R as a function of λ for tensile tests of 2AA, 8AA, 2AA30StA, and LOW at a crosshead velocity of 500 mm/min corresponding to an initial strain rate of $0.56\,s^{-1}$.

Several interesting results previously hidden in the nonlinear behavior appear more clearly from this analysis. The obtained parameters are given in Table 2 where we consider the results as a function of V_t. First of all, for all adhesives except for the LOW, C_1 is roughly independent of strain rate but C_2 always increases with strain rate. Then the second important result is that, unlike conventional crosslinked rubbers, C_2 is always higher than C_1.

Although the Mooney–Rivlin parameters are not molecularly based, they can be interpreted qualitatively in the following way: the C_1 term, which is λ independent, represents the contribution of fixed crosslink points to the modulus, whereas the C_2 term (decreasing with λ) represents the contribution of nonpermanent crosslink points such as entanglements. The polymer segments progressively become oriented in the direction of traction, and the entanglements slip so that their contribution to the modulus progressively decreases. The strain hardening at high λ is due to the finite extensibility of the polymer chains and is not taken into account by the Mooney–Rivlin model, although more advanced models consider it [32,33].

Let us now apply these molecular interpretations to our data. The first important observation is the much larger value of C_2 relative to C_1 for all adhesives. This is in contrast to conventional crosslinked rubbers [33] and shows that the PSA are entangled but weakly

TABLE 2 Coefficients C_1 and C_2 Obtained by Fitting Tensile Tests, Performed at Different Crosshead Velocities, to the Mooney–Rivlin Model (Equation 2)

V_t (mm/min)	5	50	500
		2AA	
C_1	0.0049	0.0030	0.0049
C_2	0.013	0.020	0.032
C_2/C_1	2.6	6.7	6.7
		8AA	
C_1	0.0066	0.0076	0.0120
C_2	0.037	0.043	0.110
C_2/C_1	5.6	5.6	9.1
		30StA	
C_1	0.0059	0.0072	0.0072
C_2	0.008	0.013	0.021
C_2/C_1	1.4	1.8	2.9
		LOW	
C_1		0.00078	0.00093
C_2		0.016	0.015
C_2/C_1		20.4	45.5

crosslinked systems. This is an important requirement to form fibrils, because the softening at intermediate strains makes it easy to cavitate and then to stop the growth of the cavity at the interface to make it grow in the bulk.

A second general observation is the invariance of C_1 and the increase of C_2 with strain rate. This is a signature of the viscoelastic character of the adhesive, and it is clearly the contribution of the entanglements to the modulus that is the most sensitive to the strain rate. At high strain rate, a higher density of entanglements is effective, whereas at low strain rate relaxation can take place. This effect is the most pronounced (as expected) for the LOW sample where C_2 increases by a factor of four in two decades in strain rate.

Finally, let us focus on the ratio C_2/C_1, representing the average number of entanglements between crosslink points. The 2AA and 8AA have approximately the same ratio C_2/C_1 whereas the LOW is characterized by its very low value of C_1, which reflects the low density of crosslinks and also results in a high value of C_2/C_1. Finally, the 30StA has a much lower value of C_2/C_1, which results in a much less pronounced softening at intermediate strains. These differences in behavior certainly have effects on the deformation of the adhesives upon debonding from a surface and are considered again in the discussion section.

It is important to note at this point that the values of C_1 and C_2 obtained by fitting the experimental data with the Mooney–Rivlin model are representative of the entanglements and crosslinks that act as topological constraints to deformation in the material at a given strain rate. This point is particularly important when it comes to the C_1 parameter representing crosslinks. The characterization of our networks by Soxhlet extraction showed that they all have (except for the LOW) approximately the same gel content, *i.e.*, approximately the same degree of chemical crosslinking. Yet C_1 clearly increases with AA and seems to increase slightly with StA (see Table 2). This suggests that other types of bonds, which are not easily breakable in the bulk network but can be dissolved in a good solvent, are present. Hydrogen bonds between AA groups are obvious candidates, particularly knowing that the mole fraction of AA is as high as 18% for the 8AA. On the other hand, the C_2 parameter simply represents the density of entanglements, which increases with increasing AA content and decreases with increasing StA content, as one would expect for such a bulky side group.

4. ADHESIVE PERFORMANCE

For all adhesives, the debonding process can be broken down into different stages: cavitation, growth of cavities, fibrillation, and final debonding [24]. Cavitation takes place at the beginning of the debonding process, while the stress increases (for a typical stress–strain curve see Figure 2b). For our acrylic adhesives, σ_{max} corresponds to the moment where no new cavities appear and the existing cavities grow mostly in the plane of the interface until the initial contact surface is covered with cavities. An example of this growth process is shown in Figure 9a. At this stage the load is carried by the walls between fibrils and the inside of the cavities is under vacuum [34]. On steel surfaces, coalescence between cavities is not observed, and these walls are extended in the direction of traction until they detach from the surface of the probe at nominal deformations, which can be of the order of 600–1000%. This growth of the walls occurs at a nearly constant contact area and leads to a plateau in nominal stress, which is in part due to the elasticity of the fibrils and in part to the work done against the atmospheric pressure. We define the nominal stress at the beginning of fibrillation as σ_{bf}. In some cases, especially at high temperatures, a well-defined plateau is not observed but rather a continuous decrease in stress with strain. In this case σ_{bf} is still defined as the intersection between the two different slopes, as shown on Figure 2b. The differences in debonding mechanisms are discussed in detail later.

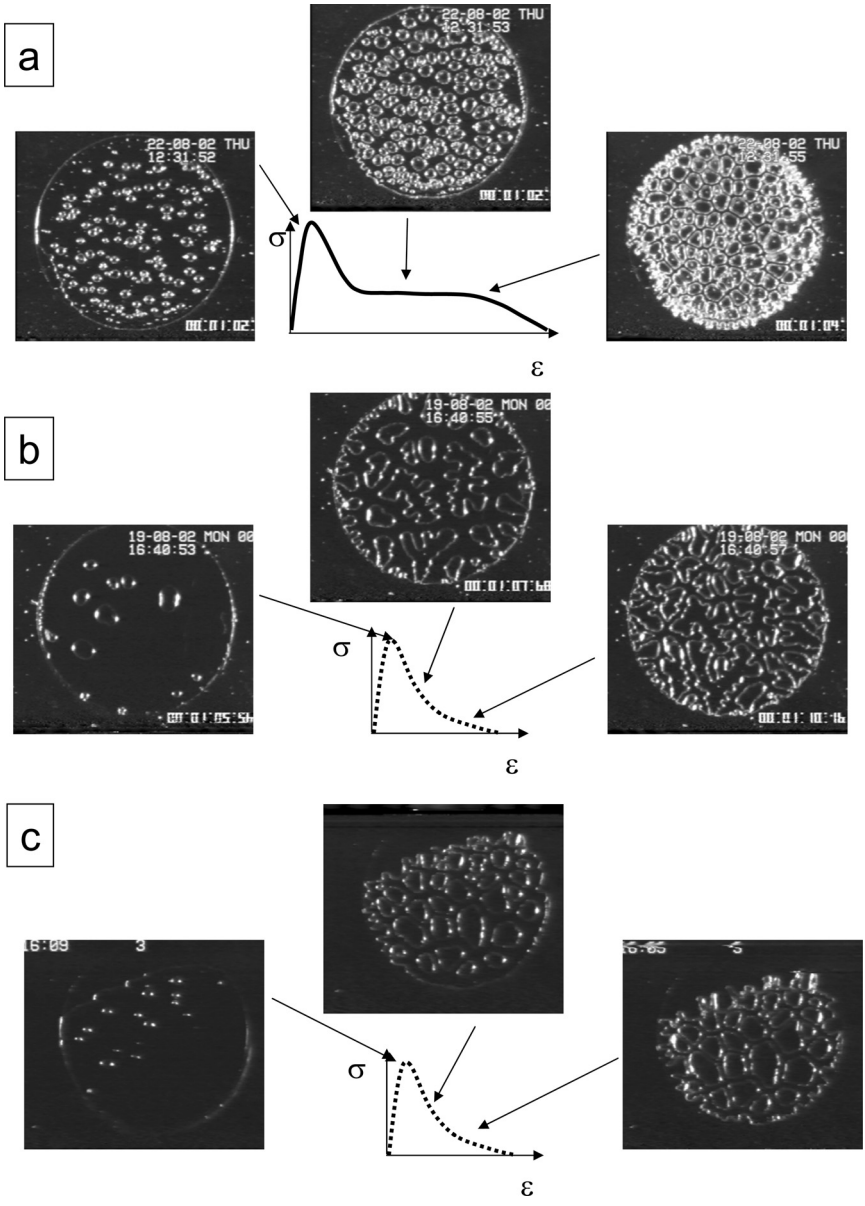

FIGURE 9 Snapshots of different debonding mechanisms and schematic drawing of the corresponding stress–strain curve: (a) example of bulk debonding (30StA, 3°C, $V_{deb} = 100\,\mu m/s$); (b) example of interfacial debonding with fingering (30StA, 60°C, $V_{deb} = 10\,\mu m/s$); (c) example of interfacial debonding without fingering (2AA, 60°C, $V_{deb} = 100\,\mu m/s$).

Eventually, the cavity walls detach from the surface of the probe and the force drops to zero at a value of deformation, which we define as ε_{max}.

As described previously, the process of debonding is rather complex, involving the nucleation of cavities under nearly hydrostatic pressure, growth of these cavities, and the formation of a fibrillar structure. Ideally, one would like to predict this type of curve from simple material properties. We explore in the following section the effect of changes in monomer composition and, to a lesser extent, degree of crosslinking on the probe test curves as well as the connection between these probe test curves and simpler material properties such as linear viscoelastic properties (Figures 3–5) and nonlinear elastic properties (Figures 6–8 and Table 2). Because the debonding process is complex, it is easier to break it down into elementary steps. Thus, after a short description of the general trends observed, we discuss the first peak in stress, focusing on the values of σ_{max} and σ_{bf}. We then discuss the fibrillation step and the values obtained for ε_{max}.

4.1. Main Trends

In this section we show typical stress–strain curves from probe tests for the different adhesives. We have chosen an intermediate debonding speed of $V_{deb} = 100\,\mu m/s$ and all results shown are at room temperature.

The nominal stress as a function of strain is represented for 2AA, 4AA, and 8AA in Figure 10, showing the effect of adding AA to the monomer composition on the adhesive properties. One clearly observes an increase in both σ_{max} and σ_{bf} with AA content, whereas the effect on the maximal elongation ε_{max} depends on the debonding velocity. One observes either a slight increase of ε_{max} with AA content for low debonding velocities ($V_{deb} = 10\,\mu m/s$) or an insensitivity to it for higher debonding velocities. The details of the mechanisms of debonding are not very dependent on the AA content and no change of the shape of the stress–strain curve is observed for the three adhesives at $V_{deb} = 100\,\mu m/s$.

When adding stearyl acrylate (Figure 11) the main consequences seen in probe tack are a decrease of the value of σ_{max} and a slight decrease of σ_{bf} for high concentrations of stearyl acrylate. Furthermore, a clear decrease of the maximal elongation ε_{max} is observed. Also in this case the form of the stress–strain curve varies little. The plateau is slightly less well defined for the high concentration of StA.

Decreasing the gel content has two opposite consequences if one targets the performance of the adhesive: a slightly lower capability

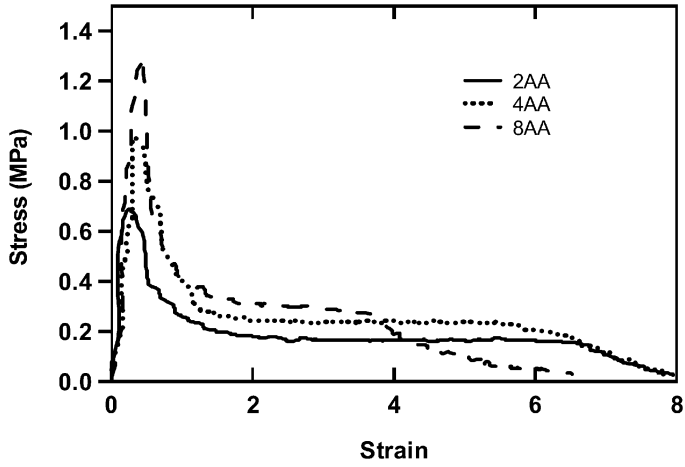

FIGURE 10 Nominal stress as a function of strain for acrylics with variable AA content. Tests performed at $V_{deb} = 100\,\mu m/s$ and room temperature.

to resist cavitation, seen in a decrease of σ_{max} and σ_{bf}, and an easier process of fibril extension, leading to a much higher value of the maximum fibril extension. This can be seen in Figure 12. It is important to note that a factor of two in the initial average molecular weight of the polymer before crosslinking (see Table 1) has a dramatic effect on the adhesive properties.

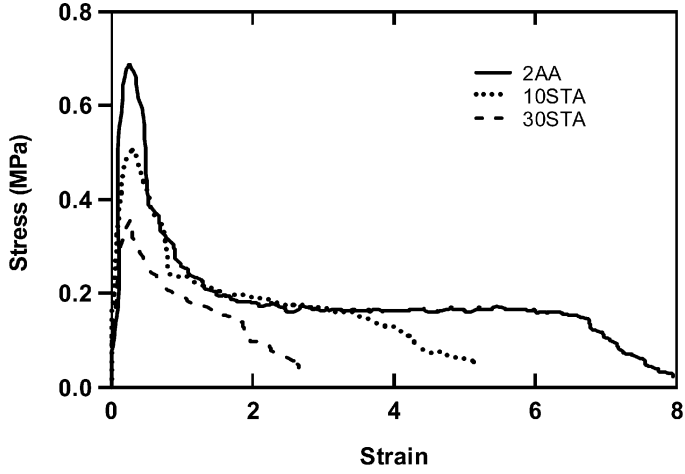

FIGURE 11 Nominal stress as a function of strain for acrylics with variable StA content. Tests performed at $V_{deb} = 100\,\mu m/s$ and room temperature.

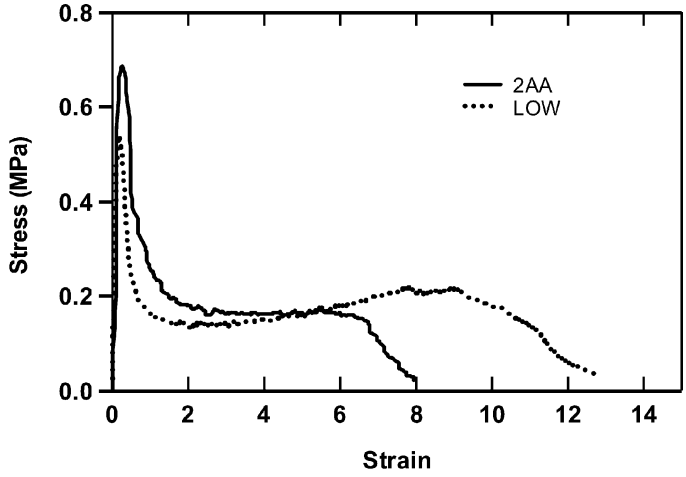

FIGURE 12 Nominal stress as a function of strain for 2AA and LOW. Tests performed at $V_{deb} = 100\,\mu m/s$ and room temperature.

4.2. The First Peak: Evolution of σ_{max} and σ_{bf}

The first peak in stress can be characterized by two main parameters, which are σ_{max} and σ_{bf}. Because this step is controlled by the resistance of the material toward cavitation, one can attempt to link these two parameters to the rheological properties of the adhesive. However, it has been proposed theoretically [35] and shown experimentally that the nucleation of cavities is strongly dependent on the presence of trapped air at the interface between the adhesive film and the probe [36,37]. Large preexisting defects (with a characteristic size larger than γ/E (the ratio between the surface tension of the adhesive and the elastic modulus of the material) cause no stress peak, whereas small defects can lead to much higher stress peaks in the probe test. Hence, σ_{max} is not really a material parameter but a complex parameter dependent on both the density and size of defects at the interface and on the viscoelastic properties of the adhesive. The same studies showed that σ_{bf}, which is characteristic of the beginning of the process of collective growth of the cavities as a foam, is independent of the way the initial adhesive/probe contact was formed [37] and might thus, be related to the material properties only. In the following, we use this result and attempt to relate σ_{max} and σ_{bf} to the linear viscoelastic properties of the adhesives and to its nonlinear elastic properties.

4.2.1. Effect of AA Content

To extend the range of experimental conditions and to compare the results with the linear viscoelastic properties of the adhesives, the tack experiments have also been performed at $T = 3°C$ and at $T = 60°C$.

We first focus on the results obtained for the peak stress σ_{max}. The debonding velocities of $V_{deb} = 10$, 100, and 1000 μm/s correspond, for the initial thickness $h_0 = 100\,\mu m$ of our adhesive films, to initial approximate strain rates of $\dot{\varepsilon} = 0.1$, 1, and $10\,s^{-1}$. We tried to build a master curve for the different velocities and temperatures by using the shift factor a_T (see Table 3) obtained from the rheological characterizations, similar to what is done for peel tests [16,18]. The result is shown for 2AA on Figure 13a. The frequency temperature superposition seems to work very well between 60°C and 22°C. However, for 3°C one observes a shift toward lower values. Qualitatively the same observations are made for 4AA and 8AA. This seems to indicate that there is a change in the debonding mechanism when going to lower temperatures that invalidates the time–temperature equivalence. As pointed out previously, it is known that the value of σ_{max} does not only depend on the rheological properties of the adhesive but is also a function of the size and a real density of initial defects present at the interface between the adhesive and the probe [37]. These initial defects are formed during the compressive contact stage, presumably by the trapping of submicron air bubbles. At 3°C, the modulus of the adhesive increases and the interface may contain larger contact defects so that

TABLE 3 Shift Factors a_T Measured from Rheological Data at 3°C and 60°C Shifts are Made Relative to the Reference Temperature of 22°C

Polymer	T (°C)	a_T
2AA	3	8.2
	60	0.097944
4AA	3	8.62
	60	0.08966
8AA	3	19.2534
	60	0.0401
10StA	3	9.805
	60	0.050462
30StA	3	
	60	0.04700
LOW	3	8.1888
	60	0.097944

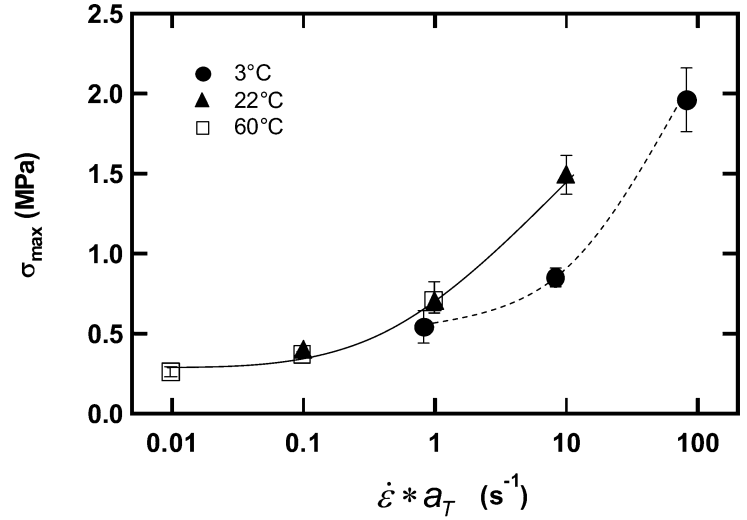

(a)

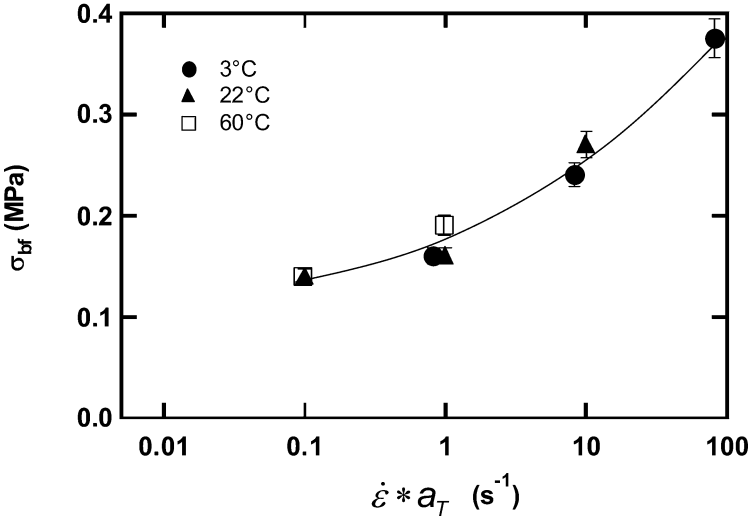

(b)

FIGURE 13 (a) Maximal stress $\sigma_{\max}$ as a function of $\dot{\varepsilon} * a_T(1/s)$ for 2AA at different temperatures: 3°C (●), 22°C (▲), and 60°C (□); (b) stress at the beginning of fibrillation σ_{bf} as a function of $\dot{\varepsilon} * a_T(1/s)$ for 2AA at different temperatures: 3°C (●), 22°C (▲) and 60°C (□).

the nucleation of cavities occurs for lower levels of average stress. On the other hand, as discussed previously, σ_{bf}, as defined in Figure 2b, is insensitive to the details of the contact formation and depends only on the material parameters of the adhesive. When representing σ_{bf} as a function of V_{deb}/h_0 (Figure 13b) one observes that the results for the different temperatures fall now on the same master curve. The successful application of the T–t superposition indicates again that σ_{bf} is a more reliable material-dependent parameter, which only depends on the viscoelastic properties of the adhesive. Thus in the following, we concentrate on the results for σ_{bf}. The master curves for 2AA, 4AA, and 8AA obtained in this way are shown in Figure 14a. From this figure it is clear that σ_{bf} increases with increasing AA content as well as with increasing strain rate. The increase with strain rate can be describes by a power law of the type $\sigma_{bf} \propto (V_{deb}/h_0)^n$ with $n \approx 0.15-0.2$. It is interesting now to check whether this dependence is related to the rheological properties of the adhesive.

In an elastic material, one expects σ_{bf} to be proportional to the stress necessary to expand an existing large cavity (in the regime where surface tension is negligible). In a viscoelastic material, the elastic modulus depends on frequency and can only be characterized at a given frequency by its storage modulus $G'(\omega)$ and loss modulus $G''(\omega)$. A reasonable representation of the instantaneous modulus is then $G^*(\omega) = (G'(\omega^2) + G''(\omega^2))^{1/2}$. To compare a rheological property at a fixed frequency with a tack test where a range of strain rates are applied to the material, we need to make an assumption about the average strain rate that the material sees during the stage where cavities form in the layer. We typically choose as approximate strain rate $\dot{\varepsilon}_{equ} = V_{deb}/h_0$ [24,25]. Because of the compliance of the apparatus, the real strain rate applied to the sample is always lower then the nominal one in the first part of the experiment and becomes higher after the peak [34,38]. In our experiments the compliance of the apparatus was of the order of 4 μm/N whereas the compliance of the layers before cavities appear was of the order of 0.2 μm/N (for the 8AA) and 0.8 μm/N (for the 2AA). Hence, the discrepancy in strain rate at the beginning of the test can be of the order of 20. However, when approaching the peak stress the compliance of the layer increases and is nearly identical to the compliance of the machine. Because it is not clear which strain rate is the most relevant to compare with the rheology, we decided to stick to the nominal strain rate.

This comparison between plateau stress and shear modulus yields two interesting results: first of all Figure 14b shows that $\sigma_{bf}(\dot{\varepsilon}_{equ})$ scales reasonably well with $G^*(\omega)$ when comparing adhesives with different AA contents. Second, $\sigma_{bf}(\dot{\varepsilon}_{equ})/G^*(\omega)$ decreases slightly with

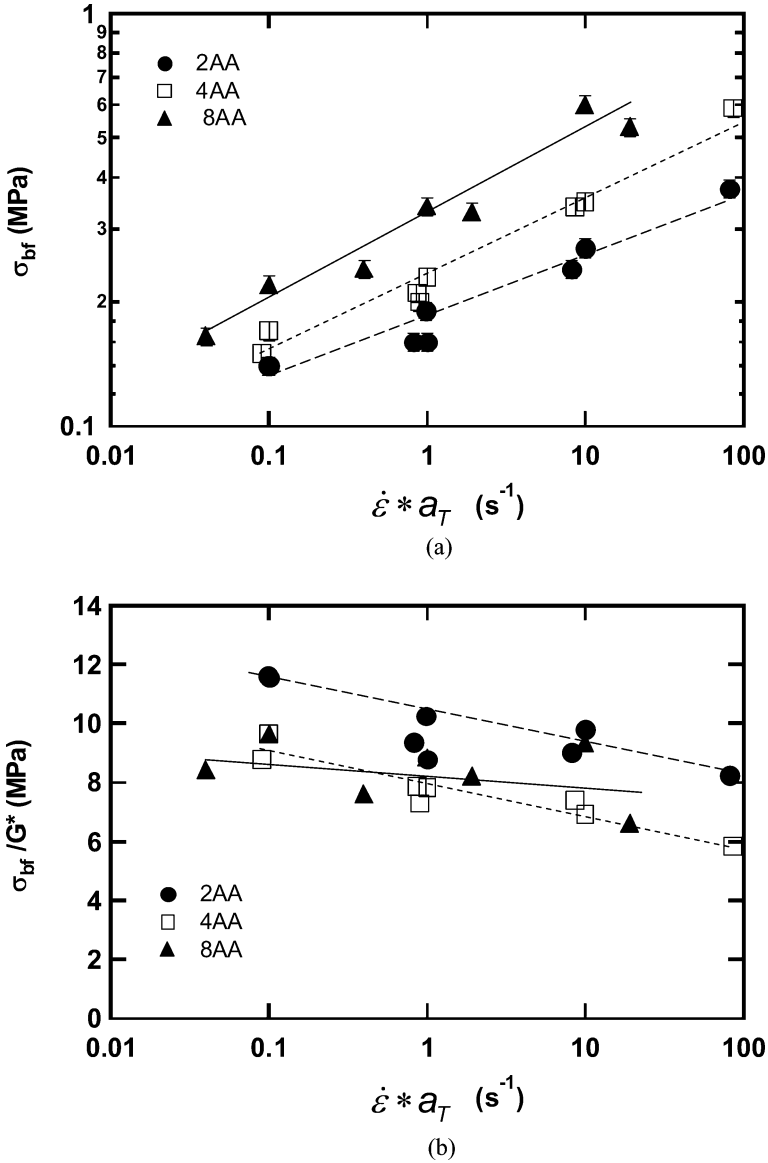

FIGURE 14 (a) Stress at the beginning of fibrillation σ_{bf} as a function of $\dot{\varepsilon} * a_T$ for acrylics with different AA content: 2AA (●), 4AA (□), and 8AA (▲); (b) ratio σ_{bf}/G^*; (c) ratio of σ_{bf} corrected by the atmospheric pressure and G^* obtained from linear rheology.

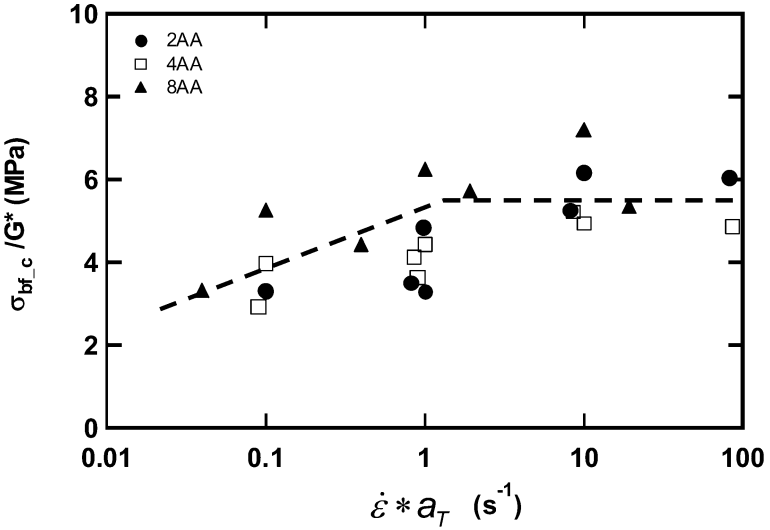

(c)

FIGURE 14 Continued.

increasing frequency. This negative slope is because at the beginning of the plateau region, the inside of the cavities is under vacuum and thus one has to work against the atmospheric pressure over the region of the probe where cavities are present. To compare the plateau stress with a material property, σ_{bf} must be decreased by ~ 0.1 MPa. Figure 14c compares the corrected value of σ_{bf} with the shear modulus G^*. A value of σ_{bf_c}/G^* close to four is now found with a slight increase of the value with frequency. This seems to indicate that the raw results were overcorrected. A systematic observation of the videos recorded during debonding show that for low frequencies and high temperatures moderate growth of fingers from the outside is observed as shown in Figure 9b. Of course, the increase in volume due to the growth of the fingers does not do any work against the atmospheric pressure.

The high frequency values of σ_{bf_c} are nearly constant at about six times G^*. This value is rather high considering that σ_{bf_c} is calculated by dividing the force by the initial contact area, while at this stage the walls only occupy a fraction of it (about 20%). In other words the walls between cavities appear to be remarkably strong relative to the shear modulus of the adhesive. This may imply that the central section of the walls is actually highly extended, in a regime where the strain hardening is important (see Figure 7) and that one would have to

consider the nonlinear rheological properties rather then the shear modulus.

4.2.2. Effect of StA Content

The same methodology can be applied for the adhesives containing the stearyl acrylate comonomer. For the 10StA and 30StA, the frequency-temperature superposition works well for σ_{bf} (Figure 15a) whereas for σ_{max} (not shown) stronger scatter of the data is observed. Thus, we directly focus on σ_{bf}. Figure 15a shows that the change in σ_{bf} is small or nonexistent when changing the StA content. Yet the incorporation of StA has a clear effect on the linear viscoelastic moduli, where one observes a decrease of G' with StA content. When comparing $\sigma_{bf}(\dot{\varepsilon}_{equ})$ with $G^*(\omega)$ the obtained scaling is clearly not satisfactory (not shown) with higher values found for 30StA and again a decrease of σ_{bf}/G^* for higher frequencies. When correcting σ_{bf} by the work done against the atmospheric pressure (Figure 15b) one obtains slightly less scatter in the values of σ_{bf_c}/G^* but in this case an increase of σ_{bf_c}/G^* with frequency, implying an overcorrection of the data that are especially pronounced for 2AA30StA. Observation of the videos demonstrates that the debonding occurs also by growth of fingers at low velocities and high temperatures. This growth is very pronounced for 30StA (see Figure 9b) and much less developed for 2AA10StA and 2AA (see Figure 9c). At low temperatures and high frequencies no finger growth is observed (see Figure 9a). This might explain why the data for 2AA30StA at low frequencies and high temperatures are overcorrected compared with the other values. Based on the high frequency data, which are the most reliable, the value of σ_{bf_c}/G^* is again around five to six for the 2AA and 2AA10StA but around 10 for the 2AA30StA. As already pointed out, in this case the values for 2AA30Sta are significantly higher than those for 2AA or 2AA10StA. We do not have a clear explanation for this discrepancy but suspect that it might be linked to the different behavior of the 2AA30StA at large strains.

4.2.3. Effect of Initial Molecular Weight and Gel Content

Figure 16a shows that σ_{bf} only varies slightly when changing the molecular-weight distribution, in agreement with the effect on linear viscoelasticity. The comparison between the uncorrected value of σ_{bf} and G^* (not shown) shows a clear decrease of σ_{bf}/G^* with frequency for the LOW. This improves very nicely when correcting the values for LOW by the atmospheric pressure (Figure 16b). As observed for the 2AA, some fingering is also observed for the LOW at high temperatures, but almost no finger formation is observed at low temperatures.

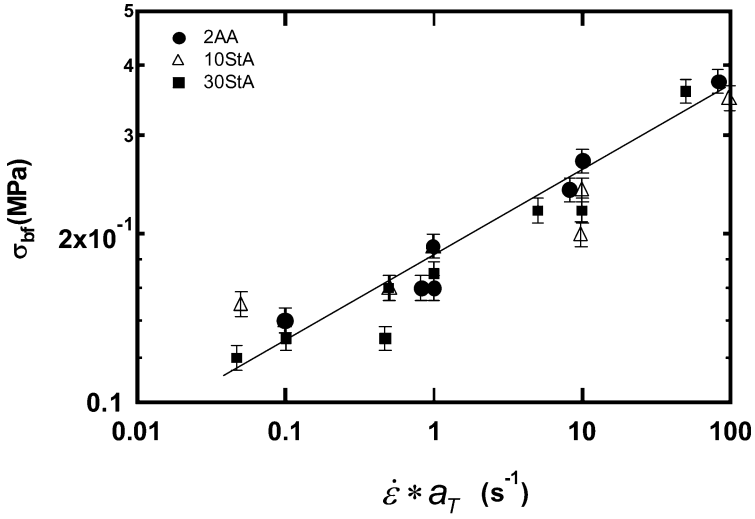

(a)

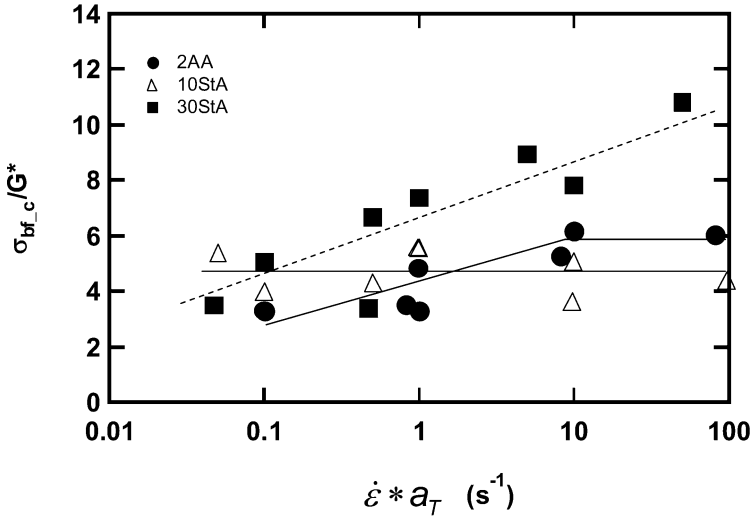

(b)

FIGURE 15 (a) Stress at the beginning of fibrillation σ_{bf} as a function of $\dot{\varepsilon} * a_T$ for acrylics with different StA content: 2AA (●), 2AA10StA (□), and 2AA30StA (▲); (b) ratio of σ_{bf} corrected by the atmospheric pressure and G^* obtained from linear rheology.

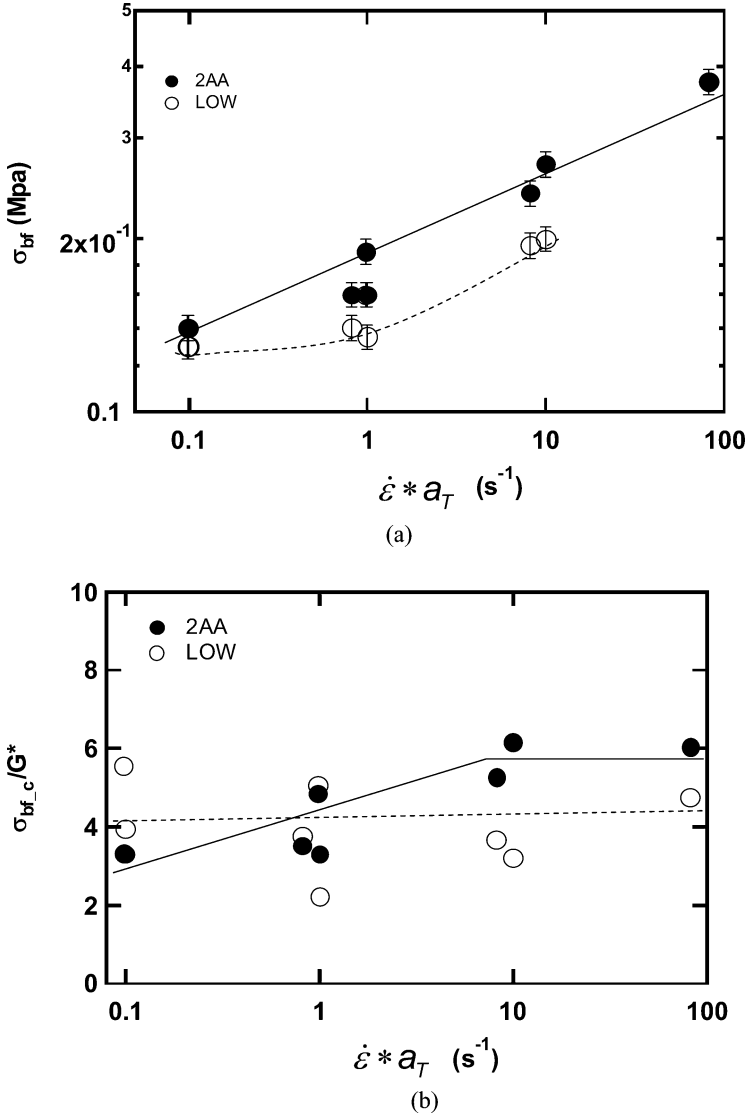

FIGURE 16 Stress at the beginning of fibrillation σ_{bf} as a function of $\dot{\varepsilon} * a_T$ for 2AA (●) and LOW (○); (b) ratio of σ_{bf} corrected by the atmospheric pressure and G^* obtained from linear rheology.

4.2.4. Summary and Comparison with Nonlinear Elasticity

In summary, these comparisons between the plateau value of the tack tests σ_{bf} and the dynamic modulus in the linear regime G^* show

that once the values of σ_{bf} have been corrected for the atmospheric pressure, all polymers have a plateau stress around five times their shear modulus or twice their tensile modulus. This implies that the stress carried by the fibrils is directly correlated with the elastic modulus of the material and that a stiffer adhesive will have a higher plateau modulus. Because the area under the plateau in stress is eventually dissipated upon final detachment of the fibrils and is a significant contribution to the work of adhesion, this is an important finding. However, the 2AA30StA adhesive is a notable exception to this rule because even after correction, the plateau in stress remains about 10 times higher than the shear modulus. Let us now examine a possible reason for this discrepancy.

At the beginning of the fibrillation step one observes extensions of the adhesive close to $\varepsilon = 1$, a deformation outside the range of validity of linear viscoelasticity. Thus, it seems more appropriate to compare σ_{bf} with the stresses obtained in the tensile test. One could attempt to directly compare the form of the stress–strain curves from the tensile tests with the stress–strain curves obtained from the tack tests at identical strain levels. However, the shape of these curves is not similar, as can be seen when comparing, for example, Figures 6 and 10. This is because debonding continues during the fibrillation step for the tack test, decreasing in this way the nominal stress.

But it is still interesting to compare the value of σ_{bf} corrected by the atmospheric pressure with the nominal stress of a simple tensile test at a typical extension ratio corresponding to the beginning of the fibrillation stage: $\varepsilon = 1$ and thus $\lambda = 2$.

Unfortunately, the tensile tests were only performed at room temperature over a narrow range of reduced frequencies. Therefore, we do not show a direct comparison but point out that the agreement between σ_{bf_c} and σ_r for 2AA and 2AA30StA is better than that between σ_{bf_c} and G^*. When comparing σ_{bf_c} and σ_r, values around three to four are found, and the nonlinear properties seem to account better for the observed values for σ_{bf_c} than the linear rheological properties.

One can conclude that when attempting to predict the onset of failure by cavitation from rheological measurements, one should concentrate on the value of σ_{bf_c}, which is a robust parameter that depends on only the material properties of the adhesive. If the strain hardening behavior is similar, σ_{bf_c} scales well with the linear viscoelastic modulus G^*. However, in the general case, a comparison with nonlinear elasticity gives better results.

It should be also pointed out that, for a meaningful comparison with material properties, raw results for σ_{bf} should be corrected for the

work done against the atmospheric pressure when cavities at nearly zero pressure are enclosed in the layer [34]. For soft solids, such as the acrylic adhesives of this study, it is not easy to predict the exact value of this correction because finger growth from the edges is observed in some cases over part of the contact zone.

4.3. Fibrillation Step: ε_{max}

Once the cavities or fingers have filled most of the volume between the two plates, *i.e.*, at $\varepsilon = 1$, they can either coalesce with each other at the interface, in which case no plateau in stress is observed, or they can start growing in size in the tensile direction. This process of extending the cavity walls in the direction of traction is often called fibrillation by analogy with elongated fibrils. However, it should be kept in mind that for most of this process the cavities are still under vacuum while the outside of the contact zone is at atmospheric pressure. As the walls are extended, the true stress in the walls undoubtedly increases. However, the measured total force on the probe (which is then normalized by the initial area of contact to give the nominal stress) can either increase, remain nearly constant, or decrease with increasing nominal strain as shown schematically in Figure 17. The final detachment of the walls will then determine the value of ε_{max}. This value depends strongly on the details of the debonding mechanism and in particular, is, a result of the interplay between the resistance to interfacial crack propagation (characterized by the critical energy release rate $\mathcal{G}_c$) and the resistance to bulk deformation (characterized by the elastic modulus $E' = 3G'$). In the limit of linearly elastic materials, the correct reduced parameter controlling the competition between coalescence of the cavities and fibrillation is $\mathcal{G}_c/Er$, where r is the projected radius

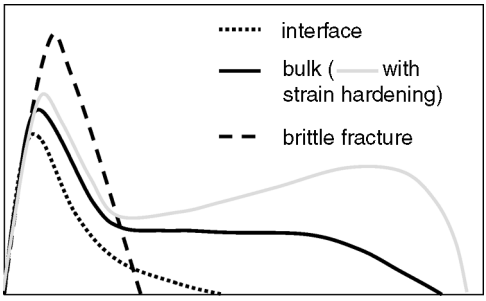

FIGURE 17 Schematic representation of the typical stress–strain curves observed for different debonding mechanisms with our adhesives.

of a penny-shaped crack representing the initial defect size, which may be estimated around 1-200 nanometers for our materials [37]. For $\mathcal{G}_c/Er > 0.5$, cavity growth in the bulk is predicted, whereas for lower values, interfacial growth should occur [23].

For viscoelastic materials deformed at large strains such as ours, this analysis is still expected to be qualitatively correct, but one expects the transition from one mechanism to another to be more progressive and to depend on temperature and debonding rate. Furthermore, the modulus may need to be replaced by a parameter more characteristic of the large strain behavior.

Because both $\mathcal{G}_c$ and E are influenced by a change in temperature, leading eventually to a change in debonding mechanisms, it is much less evident that a temperature frequency superposition should work in this case, and it seems also less likely that a simple relationship between ε_{max} and the rheological properties of the adhesives can be found.

In the following, we first describe the different types of mechanisms observed for the different adhesives as a function of debonding speed and temperature. Once we have identified these mechanisms we discuss the characteristics of ε_{max} within these groups of mechanisms.

The stress–strain curves found for the typical mechanisms observed for our adhesives are shown in a schematic way in Figure 17. All of our acrylic adhesives are crosslinked, so we do not observe the debonding mechanisms typical of fluids [34,39–41]. At room temperature, a plateau of fibrillation with a nearly constant nominal stress with deformation is observed for most of the adhesives. This constant nominal stress results from a competition between extension of the walls between cavities in the direction of traction leading to the fibrillar structure and lateral growth of the cavities leading to a shrinkage of the effective load-bearing area. Final debonding occurs by the simultaneous breakdown of the walls between cavities, entry of air, and detachment of the walls from the surface, in most of the cases leading to an immediate drop of the stress to nearly zero. No residue is found on the surface. We refer to this mechanism as "bulk" mechanism. In some cases an increase of the nominal stress with strain is observed during the fibrillation step; in this case we refer to the mechanism as "bulk with strain hardening." Snapshots of a typical bulk mechanism are shown in Figure 9a. At 60°C and low debonding velocities, this plateau vanishes, and one observes a continuous decrease of the stress with increasing strain after the initial peak. Images show a growth of the initially expanded cavities along the interface as oblate discs. No real fibrillar structure is formed, but when two adjacent cavities come very close to each other, either they coalesce or, if there is a

pressure differential, air penetrates across the thin wall. In both situations the stress drops and vanishes. The shown values of ε_{max} always correspond to this moment. We refer to this mechanism as "interface" mechanism. Snapshots of typical interfacial debonding mechanisms are shown in Figure 9b and 9c.

At low temperatures and high frequencies, exceptionally brittle fracture is observed.

As expected, the time–temperature superposition does not work very well for ε_{max} as a function of $\dot{\varepsilon} * a_T$. In the following, we discuss the results obtained for different temperatures separately. We concentrate mainly on the results obtained at room temperature but comment on a possible change of mechanisms observed when going to higher or lower temperatures.

Figure 18 summarizes the different debonding mechanisms observed for the adhesives with variable AA and StA content. For the AA series at 3°C and 22°C, the failure mechanism involves mainly bulk deformation, whereas at 60°C a clear shift toward an interfacial mechanism is observed. At room temperature ε_{max} is in the same range for the 4AA and 8AA (Figure 19). This observation is consistent with a process of extension of the fibrils mainly dominated by the strain hardening behavior at large strains, which differs little for these two adhesives (Figure 7). On the other hand, the maximum extension of the fibrils increases with $\dot{\varepsilon}$ for the 2AA, reflecting the interfacial propagation observed at low rates evolving progressively toward a bulk failure mechanism. At lower temperatures the debonding mechanisms are similar to what is observed at room temperature, except for $T = 3$°C and high debonding speeds where the 8AA adhesive fails by brittle fracture, leading to a sharp decrease of ε_{max}. At higher temperatures ($T = 60$°C) ε_{max} is generally lower for all adhesives and always increases with debonding speed. This is typical of an interfacial mechanism [25].

For the LOW, significantly larger values for ε_{max} are measured, and bulk deformation with strain hardening is observed at room temperature, suggesting that the lower degree of crosslinking plays an essential role in the process of deformation of the fibrils consistent with what was found by Zosel [42].

The situation for the StA adhesives is markedly different. Also in this case debonding at 3°C occurs mostly by bulk deformation: however, the shift toward an interfacial mechanism is already observed at 22°C where a marked difference in ε_{max} between the different adhesives and an increase of ε_{max} with debonding speed is clearly seen (Figure 20). This behavior is a signature of the interfacial debonding mechanism, which is also clearly observed with our video images

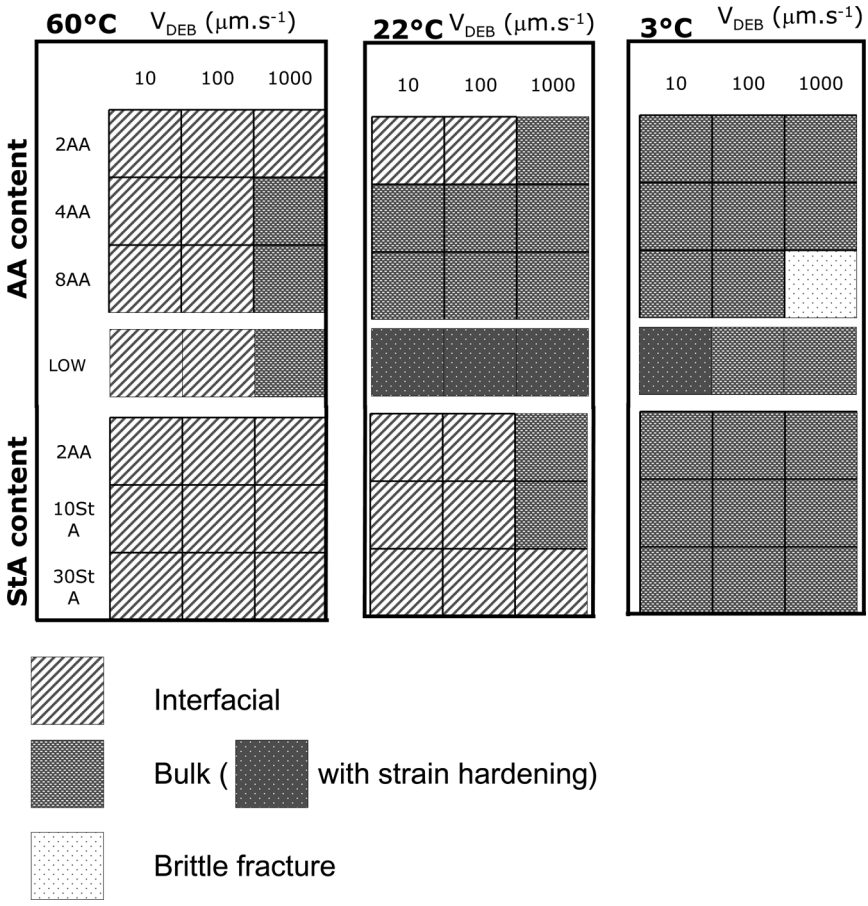

FIGURE 18 Map of the debonding mechanisms observed for our adhesives as a function of debonding rate and temperature.

(see Figure 9b or 9c). This behavior is even more pronounced for higher temperatures, where interfacial crack propagation is dominant. On the other hand, for low temperatures bulk deformation is observed and ε_{max} becomes nearly constant at a value close to what is observed for the AA series.

In summary, at low temperature and high debonding rates, the failure is brittle with low values of ε_{max}. This mechanism is only seen for 8AA. At intermediate values of debonding rates and temperatures, there exists an optimum regime where ε_{max} is nearly independent of velocity but very dependent on the extensional properties of the

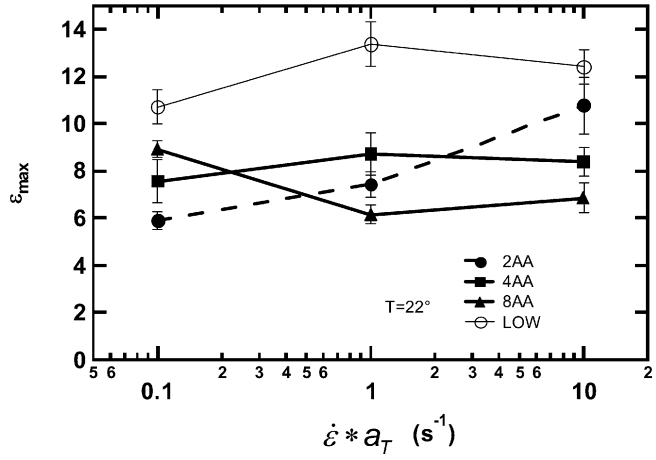

FIGURE 19 Maximal elongation ε_{max} as a function of $\dot{\varepsilon} * a_T$ for adhesives with different AA [2AA (●), 4AA (■) and 8AA (▲)] content and LOW (○) at room temperature.

adhesive. At high temperature and low debonding rates, the failure occurs through lateral propagation of cracks, and ε_{max} is low and depends on debonding rate.

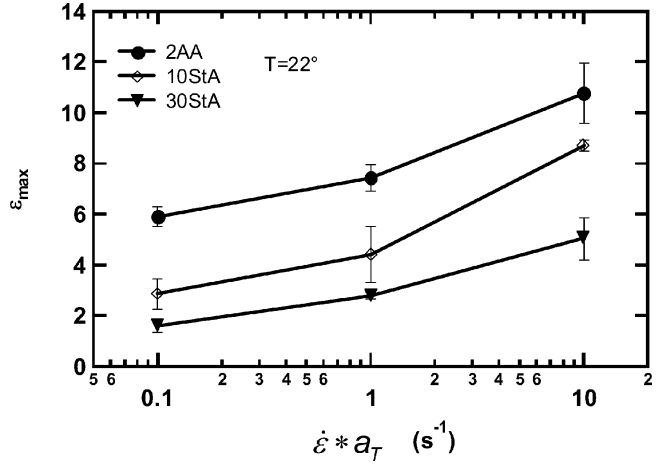

FIGURE 20 Maximal elongation ε_{max} as a function of $\dot{\varepsilon} * a_T$ for adhesives with different StA content [2AA (●), 2AA10StA (◇), and 2AA30StA (▼)] at room temperature.

4.4. Work of Adhesion

Although in this article we have emphasized a detailed analysis of the micromechanisms of debonding, it is worthwhile to discuss briefly a more macroscopic parameter that is often used in practice, such as the work of adhesion. We define the work of adhesion as the integral under the stress–strain curve multiplied by the thickness of the layer. It has the conventional units of J/m^2, although for thin confined layers W_{adh} is clearly not independent of layer thickness. Therefore this

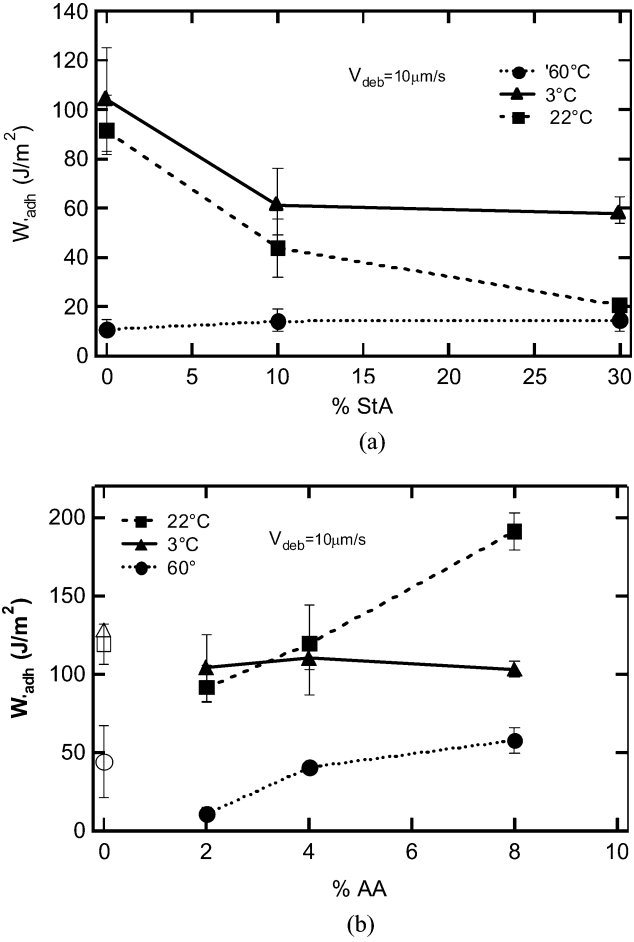

FIGURE 21 (a) Work of adhesion as a function of AA content at different temperatures: 3°C (▲), 22°C (■), 60°C (●); (b) work of adhesion as a function of StA content at different temperatures: 3°C (▲), 22°C (■), 60°C (●).

parameter should be seen as a qualitative measure of the amount of energy necessary to detach a 100-μm-thick adhesive layer from a steel substrate. Figure 21 shows quite clearly the effect of incorporating AA and StA as a comonomer in the polymer chain. The most striking effect is observed at room temperature where the addition of AA (Figure 21b) increases the work of adhesion, while the incorporation of StA (Figure 21a) decreases it significantly. For the AA at 60°C and the StA at 3°C, the effect is similar but less pronounced. However, for the 2AA at 3°C, the effect of adding AA is more complex because these materials tend to fail by brittle fracture. For the StA at 60°C, all values are low and the main contribution to W_{adh} may be the work done against the atmospheric pressure.

5. DISCUSSION

The two main stated goals of our study were as follows:

- to investigate the effect of a change in monomer composition in the adhesive and rheological properties of model acrylic PSAs, and
- to examine critically the widely used relationship between work of adhesion, which is a rather complex property and includes interfacial interactions, and rheological properties.

We first discuss the effect of monomer changes and then the relationship between rheology and work of adhesion.

The macroscopic effect of acrylic acid on the rheological and adhesive properties is quite clear. At a low concentration, the acrylic acid functions increase the magnitude of the complex modulus over a range of frequencies (Figure 3a). In probe tests, the main effect of this increase in modulus is seen in the increase in the plateau value of stress after the first peak. In other words, cavities and then fibrils are formed at higher stresses. At the molecular level, the picture is more complex: In principle the AA can form labile hydrogen bonds with itself and form stronger bonds with the Ti-chelate used to crosslink the adhesive. The exact proportion of both bonds is unknown. The presence of hydrogen bonds will not be seen in the gel content because they can be dissolved but will affect the nonlinear elastic properties of the network.

Several authors have noted that the sol fraction of the polymer containing AA can migrate toward the interface with the substrate and increase the level of interfacial interactions with the surface beyond van der Waals forces [4,43]. However, this migration is reported to occur in hours and at the 1-s contact times that we use it is unlikely that significant segregation of AA at the interface is observed.

At higher AA content (8 wt% but 18 mol%), the glass transition temperature is also increased, making the adhesive more dissipative at room temperature. It is likely that this increase in dissipative character is the main reason for the increase in $\mathcal{G}_c$ that we observe.

The macroscopic effect of adding StA has been much less studied and is more complex. In terms of modulus, adding 10% of StA has very little effect, whereas at 30% the dominant effect is a decrease in modulus. In probe tests the addition of the StA comonomer decreases the peak stress and plateau level and overall reduces the work of adhesion by shortening the plateau significantly.

In this case at the molecular level, the crosslinking density should in principle remain the same because the AA content and Ti-chelate remains the same. However, the nonlinear elastic properties indicate a higher density of crosslinks for the 2AA30StA, the origin of which is unknown. On the other hand, the larger size of the StA comonomer means also that the average molecular weight between entanglements of the copolymer increases slightly. This effect is highly apparent in the 2AA30StA copolymer, which is less entangled. The effect of this change leads to a lower level of adhesion but a direct interpretation in terms of molecular structure is difficult and can only be discussed with the help of both linear and nonlinear rheology. The effect of adding stearyl acrylate on interfacial interactions should be neutral on a high-energy surface such as steel, because the only difference is a slightly lower surface energy for StA relative to E2HA. Furthermore, at least at small strains, the 2AA30StA is not more dissipative than the 2AA (see Figure 4b). Yet the observed $\mathcal{G}_c$ is clearly lower for the high StA networks, implying that the dissipative processes occurring at the interface upon crack propagation are not simply related to tan δ.

A recurring question when studying adhesion of soft materials is the relationship between the viscoelastic properties of the material and the work of adhesion. One of the oldest conjectures widely used in the adhesion community is to make a direct link between the rheological properties of the adhesive itself and the measured adhesion [44–46]. This conjecture was originally made because it is very often possible to construct adhesive master curves with peel tests performed at different temperatures and peel rates. A modification of a characteristic relaxation time of the material often leads to a proportional shift in the adhesive master curve, therefore stressing the importance of the relaxation time of the adhesive on the work of debonding [16,47].

However, because of the rather complex and inhomogeneous deformation field during fracture, it is much more difficult to quantitatively relate the amount of dissipated energy to a specific viscoelastic parameter typically obtained at a fixed frequency and in the linear

regime. In our analysis we have tried to go beyond this simple correlation work by studying not the peel force but the details of the force-displacement curve obtained in a probe test and critically examining how a rheological measurement performed on materials deformed homogeneously can be useful to more quantitatively predict a complex deformation process.

In the main body of the article we divided our experimental results into stages: cavitation, lateral propagation, and fibril extension.

We confirm the results of Chiche *et al*. [37] that the peak stress obtained in probe tests is only a reliable material parameter when the contact stage (for different adhesive materials) leaves at the interface defects of comparable sizes. In the general case, σ_{bf} is a much better material parameter to use to compare different adhesive materials. σ_{bf} is well predicted by the linear viscoelastic properties of the adhesives as long as the nonlinear elastic properties are not too different. For the AA series, the ratio between plateau stress and elastic modulus G^* falls around five to six when a suitable correction for the work done against atmospheric pressure is applied. On the other hand, it is about 10 for the 2AA30 StA.

The second important aspect is the lateral growth of cavities along the interface. This interfacial growth is controlled by the interplay between the storage modulus E′, the defect size r, and the energy-release rate $\mathcal{G}_c$. At low debonding rates and high temperatures, the value of $\mathcal{G}_c$ is typically low and E and r remain roughly constant. At intermediate debonding rates and temperatures, $\mathcal{G}_c$ increases faster than E with increasing debonding rate, r remains constant, and $\mathcal{G}_c/Er$ then reaches a maximum. In this regime, fibrils form and their extension is controlled by the elongational properties of the adhesive only (see the next section). At low temperatures, $\mathcal{G}_c$ stays high but r starts to increase because the high effective modulus of the adhesive at low temperature prevents the adhesive from conforming perfectly to the surface of the probe. Because E increases, $\mathcal{G}_c/Er$ decreases again, and the mechanism shifts from bulk fibrillar to brittle interfacial. This scenario is rather general for all soft viscoelastic materials. Of course, what varies is the time/temperature domain where these different regimes are observed and the absolute value of the work of adhesion in the domain of maximum adhesion, which is controlled by the nonlinear viscoelastic properties of the material.

In the specific case of the model adhesives of this study, the shift in mechanism between interfacial propagation and bulk deformation corresponding to the point where interfacial propagation is minimized is reached at different velocities/temperatures. For the 4AA and 8AA, at 60°C and 1000 μm/s the bulk mechanism kicks in, whereas for the 2AA

and 2AA10 StA, it is only at 22°C and 1000 μm/s, and for the 2AA30 StA it is at 3°C and 10 μm/s.

This can be interpreted in the following way: both $\mathcal{G}_c$ and E increase with increasing AA content: however, the increase in $\mathcal{G}_c$ dominates, so that $\mathcal{G}_c/Er$ increases with increasing AA content, leading to a bulk mechanism at lower frequencies/higher temperatures. Following the same analysis, an increase in StA leads to a decrease of $\mathcal{G}_c$ and E, but the decrease in $\mathcal{G}_c$ still dominates over the decrease in E, so that $\mathcal{G}_c/Er$ decreases with increasing StA content, leading to interfacial crack propagation.

In both cases the implication of our results is that the chief effect of adding the comonomer is to change the resistance to crack propagation $\mathcal{G}_c$, with AA increasing $\mathcal{G}_c$ and StA decreasing $\mathcal{G}_c$.

The situation is fundamentally different when comparing low and high molecular weight. In this case, the extensional properties differ strongly, leading to different plateau values of ε_{max}, and the transition between interfacial and bulk mechanism does not occur for the same conditions as the for the 2AA, even though both small strain modulus and AA content are identical.

For this case, it is essential to take into account the nonlinear elastic behaviour. Although in the linear regime at low strains our model adhesives are quite viscoelastic, this is no longer true at large strains where the crosslinking structure imposes a less strain-rate-dependent behavior. In this large strain regime, we found (Figure 8) that the stress–strain curve can be approximately fitted by the Mooney–Rivlin model. From this model, two parameters C_1 and C_2 are extracted. The shear modulus in the linear regime is given by the value of $2(C_1 + C_2)$. Because C_2 is larger than C_1 in all adhesives it is reasonable to say that the value of C_2 mainly controls the small strain behavior of the adhesive and hence its resistance to cavitation and initial level of plateau stress. On the other hand, the ratio C_2/C_1 controls the evolution of the stress–strain behavior in large strain, and this will have a direct effect on the shape of the plateau in stress observed in probe tests.

With these tools we can now address the question of the control of the fibril extension by the nonlinear elastic properties of the adhesive.

2AA has a C_2/C_1 value around five. This type of crosslinking corresponds to a general-purpose permanent adhesive. If the adhesive is more crosslinked relative to its small strain modulus, the plateau stress becomes shorter and interfacial propagation of cracks becomes dominant. This is typical for removable adhesive applications and is observed for the 30 StA adhesive ($C_2/C_1 \sim 1$–3). On the other hand if, the adhesive is less crosslinked, fibrils may become more extended but the stress level is lower. This is observed to a small extent for the

8AA ($C_2/C_1 \sim 5$–10) and to a much larger extent for the LOW ($C_2/C_1 \sim 20$–50). A slight undercrosslinking leads to an optimization of the peel force relative to the resistance to shear whereas a significant undercrosslinking will be beneficial on low energy surfaces but gives a weak resistance to shear.

Of course, this reasoning on the large strain behavior completely ignores interfacial interactions and $\mathcal{G}_c$. Yet it is likely that a good predictive model of the maximum extension of the fibrils must include both the interfacial interactions and $\mathcal{G}_c$ in some way because the foot of the fibrils need to be detached at the end. In the situation where fibrils are fully formed (*i.e.*, a true plateau in stress is observed in the probe test curve), unless changes in $\mathcal{G}_c$ are large, the highly nonlinear strain hardening brought about by the finite extensibility of the polymer chains between permanent crosslinks should be the most important parameter controlling ε_{max}. However, when a decreasing plateau in stress or a shoulder is observed in the probe test curve, ε_{max} will be controlled by the competition between nonlinear elasticity and $\mathcal{G}_c$, and a proper model of this mechanism is beyond our capability.

6. CONCLUSION

The stated goal of our investigation was twofold: first to investigate, with the most advanced methods, the effect on the material properties, of incorporating a highly polar comonomer and a nonpolar, low-surface-tension comonomer in a standard acrylate homopolymer typically used for soft adhesives; and second, to investigate the complex relationship between the viscoelastic properties of the adhesive and its adhesive properties on a substrate. The main conclusions of our study are the following:

At fixed gel fraction and molecular-weight distribution, the addition of acrylic acid increases both the elastic modulus and the resistance to interfacial crack propagation of the acrylic networks. However, a more detailed analysis of the debonding mechanisms suggests that the increase in the resistance to crack propagation $\mathcal{G}_c$ with increasing AA content is the dominant effect at low debonding rates/high temperatures whereas the increase in elastic modulus with increasing AA content becomes dominant at high rates/low temperatures.

The addition of stearyl acrylate as a comonomer reduces both the small strain modulus of the acrylic network and its resistance to interfacial crack propagation. A detailed analysis of the debonding mechanisms and of the rheological properties of the adhesives suggests that the decrease in $\mathcal{G}_c$ with increasing StA content is the dominant effect at room temperature and at high rates/low temperatures.

Surprisingly the addition of StA introduces a higher density of apparent crosslinks, which causes a more pronounced strain hardening of the adhesive at lower extensions than for the network that does not contain StA.

For most adhesives where probe tests showed a well-defined plateau in stress after the first tensile peak, the stress level of the plateau could be reasonably well predicted by the small strain modulus G^* and the measured ratio between plateau stress and shear modulus is around five to six.

The type of debonding mechanism observed (interfacial crack propagation or bulk cavitation followed by fibril extension) can be well predicted by the reduced variable $\mathcal{G}_c/Er$. However, a prediction of the absolute value of the adhesion energy from the rheological properties of the adhesive remains a difficult unsolved problem.

When the debonding mechanism involves the formation of fibrils and is clearly in the bulk, the maximum fibril extension is closely connected with the large strain nonlinear elastic properties of the adhesives. It is found that the ratio C_2/C_1 of the two Mooney–Rivlin parameters is a very good descriptor of the aptitude of the fibrils to extend. A high value of this ratio corresponds to high values of ε_{max} whereas a low value of C_2/C_1 corresponds to low values of ε_{max}.

ACKNOWLEDGMENTS

We gratefully acknowledge funding from the European 5th Framework Programme GROWTH, Contract G5RD-CT 2000-00202.

REFERENCES

[1] Creton, C., *MRS Bulletin* **28**, 434–439 (2003).
[2] Satas, D. Ed., *Handbook of Pressure Sensitive Adhesive Technology* (Van Nostrand Reinhold, New York, 1989), Vol. 1, p. 940.
[3] Ewins, E. E., St. Clair, D. J., Erickson, J. R., and Korcz, W. H., Thermoplastic Rubbers: A-B-A Block Copolymers, in *Handbook of Pressure-Sensitive-Adhesive Technology*, D. Satas (Ed.) (Van Nostrand Reinhold, New York, 1989), Vol. 1, pp. 317–373.
[4] Aubrey, D. W. and Ginosatis, S., *J. Adhes.*12, 189–198 (1981).
[5] Chan, H. and Howard, G. J., *J. Adhes.* **9**, 279–301 (1978).
[6] Dale, W. C., Paster, M. D., and Haynes, J. K., *J. Adhes.* **31**, 1–20 (1989).
[7] Mayer, A., Pith, T., Hu, G. -H., and Lambla, M., *J. Polym. Sci. B Polym. Phys.* **33**, 1781–1791 (1995).
[8] Tobing, S. D. and Klein, A., *J. Appl. Polym. Sci.* **76**, 1965–1976 (2000).
[9] Gower, M. D. and Shanks, R. A., *Macromol. Chem. Phys.* **205**, 2139–2150 (2004).
[10] Aymonier, A., Papon, E., Castelein, G., Brogly, A., and Tordjeman, P., *J. Coll. Int. Sci.* **268**, 341–347 (2003).

[11] Tobing, S., Klein, A., Sperlinh, L. -H., and Petrasko, B., *J. Appl. Polym. Sci.* **81**, 2109–2117 (2001).
[12] Tobing, S. D. and Klein, A., *J. Appl. Polym. Sci.* **79**, 2558–2564 (2001).
[13] Tobing, S. D. and Klein, A., *J. Appl. Polym. Sci.* **79**, 2230–2244 (2001).
[14] Gower, M. D. and Shanks, R. A., *Macromol. Chem. Phys.* **206**, 1015–1027 (2005).
[15] Zosel, A. and Schuler, B., *J. Adhes.* **70**, 179–195 (1999).
[16] Derail, C., Allal, A., Marin, G., and Tordjeman, P., *J. Adhes.* **61**, 123–157 (1997).
[17] Benyahia, L., Verdier, C., and Piau, J. M., *J. Adhes.* **62**, 45–73 (1997).
[18] Gent, A. N. and Petrich, R. P., *Proc. Roy. Soc. London, A* **310**, 433–448 (1969).
[19] Christensen, S. F., Everland, H., Hassager, O., and Almdal, K., *Int. J. Adhes. Adhesives* **18**, 131–137 (1998).
[20] Urahama, Y., *J. Adhes.* **31**, 47–58 (1989).
[21] Chiche, A., Zhang, W. H., Stafford, C. M., and Karim, A., *Measurement Science & Technology* **16**, 183–190 (2005).
[22] Kramer, E. J. and Berger, L. L., *Adv. Polym. Sci.* **91**/**92**, 1–68 (1990).
[23] Shull, K. R. and Creton, C., *J. Polym. Sci. B Polym. Phys.* **42**, 4023–4043 (2004).
[24] Lakrout, H., Sergot, P., and Creton, C., *J. Adhes.* **69**, 307–359 (1999).
[25] Brown, K., Hooker, J. C., and Creton, C., *Macromol. Mat. and Eng.* **287**, 163–179 (2002).
[26] Roos, A., Ph.D. thesis, Université Paris VI Paris (2004), p. 350.
[27] Daoulas, K., Theodorou, D. N., Roos, A., and Creton, C., *Macromolecules* **37**, 5093–5109 (2004).
[28] Roos, A. and Creton, C., *Macromol. Symp.* **214**, 147–156 (2004).
[29] Creton, C. and Lakrout, H., *J. Polym. Sci. B Polym. Phys.* **38**, 965–979 (2000).
[30] Lin, Y. Y., Hui, C. Y., and Conway, H. D., *J. Polym. Sci. B Polym. Phys.* **38**, 2769–2784 (2000).
[31] Cheng, L., Xia, X., Yu, W., Scriven, L. E., and Gerberich, W. W., *J. Polym. Sci. B Polym. Phys.* **38**, 10–12 (2000).
[32] Treloar, L. R. G., *Rep. Prog. Phys.* **36**, 755–826 (1973).
[33] Treloar, L. R. G., The General Strain: Phenomenological Theory, in *The Physics of Rubber Elasticity* (Clarendon Press, Oxford, 1975), pp. 210–310.
[34] Poivet, S., Nallet, F., Gay, C., Teisseire, J., and Fabre, P., *Eur. Phys. J. E* **15**, 97–116 (2004).
[35] Gay, C. and Leibler. L., *Phys. Rev. Lett.* **82**, 936–939 (1999).
[36] Chiche, A., Pareige, P., and Creton, C., *C. R. Acad. Sci. Paris, IV* **1**, 1197–1204 (2000).
[37] Chiche, A., Dollhofer, J., and Creton, C., *Eur. Phys. J. E* **17**, 389–401 (2005).
[38] Chiche, A., Ph.D. thesis, Université Paris VII Paris (2003).
[39] Derks, D., Lindner, A., Creton, C. and Bonn, D., *J. Appl. Phys*.93, 1557–1566 (2003).
[40] Tirumkudulu, M., Russell, W. B., and Huang, T. J., *Phys. Fluids* **15**, 1588–1605 (2003).
[41] Lindner, A., Derks, D., and Shelley, J. M., Stretch flow of thin layers of newtonian liquids: Fingering patterns and lifting forces, *Phys. Fluids*, **17**, (2005).
[42] Zosel, A., *Int. J. Adhes. Adh.* **18**, 265–271 (1998).
[43] Satas, D., Acrylic Adhesives, in *Handbook of Pressure-Sensitive-Adhesives*, D. Satas (Ed.) (Van Nostrand Reinhold, New York, 1989), Vol. 1, pp. 396–456.
[44] Gent, A. N. and Schultz, J., *J. Adhes.* **3**, 281–294 (1972).
[45] Andrews, E. H. and Kinloch, A. J., *Proc. Roy. Soc. London, A* **332**, 385–399 (1973).
[46] Andrews, E. H. and Kinloch, A. J., *Proc. Roy. Soc. London A* **332**, 401–414 (1973).
[47] Lakrout, H., Creton, C., Ahn, D., and Shull, K. R., *Macromolecules* **34**, 7448–7458 (2001).